Modifying macrophages at the periphery has the capacity to change microglial reactivity and to extend ALS survival

Aude Chiot, Sakina Zaïdi, Charlène Iltis, Matthieu Ribon, Félix Berriat, Lorenzo Schiaffino, Ariane Jolly, Pierre de la Grange, Michel Mallat, Delphine Bohl, et al.

Modifying macrophages at the periphery has the capacity to change microglial reactivity and to extend ALS survival

Aude Chiot[1], Sakina Zaïdi[1], Charlène Iltis[1], Matthieu Ribon[1], Félix Berriat[1], Lorenzo Schiaffino[1,2], Ariane Jolly[3], Pierre de la Grange[3] Michel Mallat[1], Delphine Bohl[1], Stéphanie Millecamps[1], Danielle Seilhean[1,4], Christian S. Lobsiger[1], Séverine Boillée[1*].

[1]Sorbonne Université, Institut du Cerveau – Paris Brain Institute, ICM, Inserm, CNRS Paris, France.

[2]Dept. of Neurological, Biomedical and Movement Science; University of Verona; Strada Le Grazie 8 - 37134 Verona, Italy.

[3]Genosplice, Paris, France

[4]Département de Neuropathologie, APHP, Hôpital Pitié-Salpêtrière, F-75013 Paris, France

* E-mail: severine.boillee@upmc.fr

Abstract:

Microglia and peripheral macrophages have both been implicated in amyotrophic lateral sclerosis (ALS), although their respective roles have yet to be determined. We now show that macrophages along peripheral motor neuron axons in mouse models and patients with ALS react to neurodegeneration. In ALS mice, peripheral myeloid cell infiltration into the spinal cord was limited and depended on disease duration. Targeted gene modulation of the reactive oxygen species pathway in peripheral myeloid cells of ALS mice, using cell replacement, reduced both peripheral macrophage and microglial activation, delayed symptoms and increased survival. Transcriptomics revealed that sciatic nerve macrophages and microglia reacted differently to neurodegeneration, with abrupt temporal changes in macrophages and progressive, unidirectional activation in microglia. Modifying peripheral macrophages suppressed proinflammatory microglial responses, with a shift toward neuronal support. Thus, modifying macrophages at the periphery has the capacity to influence disease progression and may be of therapeutic value for ALS.

Introduction

ALS is the most common of the motor neuron (MN) diseases and is characterized by the degeneration of both upper and lower MNs, leading to progressive paralysis and death of the patient. Although mainly sporadic, 10% of the cases are familial, with mutations identified in more than 25 genes (mainly autosomal dominant and ubiquitously expressed), including *C9orf72*, *SOD1*, *FUS* and *TARDBP*. *SOD1*, which encodes the Cu/Zn superoxide dismutase, is the second most frequent known cause of familial ALS[1]. Mouse models expressing mutant *SOD1* recapitulate key clinical signs of patients with ALS[2,3]. ALS is a non-cell autonomous disease, in which glial cells, in particular microglia, participate in MN degeneration[3–8]. Removing mutant SOD1 from microglia, the macrophages of the CNS, slows disease progression in ALS mice and extends survival[3,7,8]. However, in all these previous studies, the effect was attributed to microglia alone even though the myeloid lineage (monocytes, macrophages and microglia) was manipulated as a whole; therefore, the individual contributions of macrophages at the periphery and microglia in the CNS could not be discriminated[3,7–9]. Spinal MNs are unusual neurons since their soma, within the spinal cord, are surrounded by microglia while their axons, extending into the periphery, are surrounded by peripheral macrophages. Axonal pathology happens early in ALS, both in humans and mice, and is accompanied by macrophage activation in the sciatic nerve of ALS mice[10–12]. Since microglia (of yolk sac origin) and peripheral macrophages (of mostly fetal liver/bone marrow (BM) origin) have different developmental origins but also act in different environments[13–15], we hypothesized that they could promote distinct effects in ALS.

A key debated point in ALS concerns the potential of BM-derived-monocytes/macrophages to infiltrate the CNS during disease. The use of irradiation to induce myeloablation before BM transplantation leads to the infiltration of peripheral immune cells into the CNS of ALS mice. However, this effect was subsequently interpreted as a consequence of irradiation since parabiosis (an alternative to irradiation/BM grafting) showed no such infiltration into the spinal cords of ALS mice (although this was analyzed at a unique symptomatic time point)[16–20]. While specific markers for microglia versus CNS-infiltrating, blood-monocyte-derived peripheral macrophages have been identified[21–25], the maintenance of such specific markers is challenging in pathological conditions. Thus, the presence and impact on disease of such presumed CNS-infiltrated peripheral monocytes remain controversial[19–22,25].

Independent of whether or not blood-monocyte-derived macro- phages infiltrate the affected CNS in ALS, here, we characterize in detail monocytes/macrophages directly at the periphery, along the peripheral nerves containing the axons of spinal MNs, and assess their disease-modifying capacity. Regarding therapeutic perspectives, we assume that replacing and modulating these macrophages would be easier than targeting microglia in the CNS.

RESULTS

Macrophages along peripheral axons of MNs are activated in ALS mouse models and in patients with ALS. We assessed peripheral macrophage activation along sciatic nerves using CD11b, CD68 and F4/80 antibody mixtures (Fig. 1a–e and Extended Data Fig. 1a–e) in ALS mouse models that exhibit slow disease progression (SOD1^{G37R}, death at 14 months) or fast disease progression (SOD1^{G93A}, death at 5.5 months). Macrophages showed enlarged cell bodies (Fig. 1b–e), increased numbers already in presymptomatic SOD1^{G93A} mice (Fig. 1f) and increased immunoreactive areas in both lines from disease-onset onwards (Fig. 1g). There was low macrophage activation in 6-month-old mice harboring human wild-type SOD1 (hSOD1^{WT}), which is consistent with neuronal stress in this line (Fig. 1f,g).

To assess microglia and peripheral macrophage activation in human ALS compared to controls, spinal cords with ventral (motor) and dorsal (sensory) nerve roots and peripheral nerves were stained for the microglial/macrophage marker CD68 (Fig. 1h–s and Extended Data Fig. 1f–j). Eleven patients (7 patients with familial ALS with mutations in *C9orf72*, *SOD1*, *TARDBP* or *UBQLN2* and 4 patients with sporadic ALS; clinical data are provided in Supplementary Table 1) and 4 controls were included. CD68^{+} cells were present in ALS spinal cord ventral horns (Fig. 1h,k,n) and in ventral roots (Fig. 1j,m,p) and peripheral nerves (Fig. 1q) of patients with ALS, but not of controls (Fig. 1r,s and Extended Data Fig. 1f,h–j), and were rare in dorsal roots (Fig. 1i,l,o and Extended Data Fig. 1g). This result shows that there is activation/infiltration of peripheral nerve macrophages and that it is not restricted to SOD1-linked ALS.

CNS infiltration of peripheral myeloid cells depends on disease progression but remains low in ALS mice. To analyze the impact of peripheral macrophages on disease, independent of microglia, we needed to replace myeloid cells at the periphery without targeting CNS microglia and to assess whether they remained at the periphery or infiltrated the CNS. We induced myeloablation with the chemotherapy agent busulfan (at 50 days) followed by BM transplantation (whereby the BM cells expressed (green fluorescent protein (GFP)) in control mice and compared it to irradiation (Extended Data Fig. 2a). Busulfan treatment led to efficient BM aplasia and replacement of blood leukocytes at 12 days after transplantation (Extended Data Fig. 3a–d). It enabled the sustained replacement of more than 90% of blood monocytes/macrophages (CD11b^{+}F4/80^{+}) (Fig. 2a and Extended Data Fig. 3c). While irradiation led to the spinal cord infiltration of peripheral GFP^{+} myeloid cells as previously described[20], this was not the case with busulfan (Fig. 2b). Thus, SOD1^{G93A} (at 7–8 weeks) and SOD1^{G37R} (at 12–13 weeks) ALS mice were myeloablated with busulfan (Extended Data Figs. 2b,c and 3e) at the presymptomatic stage and then grafted with GFP-expressing BM (busulfan/BM transplantation) to generate GFP→SOD1^{G93A} and GFP→SOD1^{G37R} mice, respectively. CD11b^{+} blood-cell replacement was as efficient as in control mice, reaching ≥95% at disease onset for both lines (102 and 247 days, respectively)

(Extended Data Fig. 3f,g). Sciatic nerve macrophage replacement reached 70% and 75% in GFP→SOD1^{G93A} and GFP→SOD1^{G37R} mice, respectively (Fig. 2c–e) at disease onset, which is in line with nerve macrophages originating from BM precursors[26], and 70% in gastrocnemius muscles (Extended Data Fig. 3h).

The presence of GFP^+ (BM-derived) and GFP^+Iba1^+ cells (monocyte-derived macrophages) in the spinal cord was measured throughout disease. They were minimal in $SOD1^{G93A}$ mice, with a slight variable peak of 8.17 ± 4.29% GFP^+Iba1^+ cells at the late-symptomatic stage (Fig. 2f–h and Supplementary Fig. 1). In $SOD1^{G37R}$ mice, the GFP^+ area remained small (<10%, Fig. 2g), but the number of GFP^+Iba1^+ cells was higher at the early-symptomatic stage and at the end-stage, when it reached 28.5 ± 1.8% (Fig. 2f–h and Supplementary Fig. 1). GFP^+ cells were mainly localized in the ventral horn, and GFP^+ macrophages ($Iba1^+$) proliferated ($Ki67^+$) more than non-GFP endogenous microglia (Fig. 2i), which indicates that the increased number of GFP^+Iba1^+ cells resulted from both infiltration and local proliferation.

To confirm this low infiltration using a noninvasive method (compared to BM grafting), we sought markers that are specific for peripheral monocytes/macrophages and do not stain microglia. We used anti-CD169 antibodies (also known as Siglec-1, which was previously shown to be specific for peripheral macrophages[25]) in spinal cords of $SOD1^{G93A}$ mice throughout disease and of GFP→$SOD1^{G93A}$ mice at the late-symptomatic stage. However, anti-CD169 antibodies could not differentiate endogenous microglia from infiltrated peripheral myeloid cells (Extended Data Fig. 4). We then used two different reporter mice (transgenic *Ccr2*–GFP and knock-in *Ccr2*–RFP) expressing fluorescent proteins (green or red, respectively) under the *Ccr2* promoter, which is known to be expressed by monocytes and lymphocytes but not by microglia. In sciatic nerves after a crush injury, Ccr2-expressing cells in *Ccr2*–RFP mice were mainly lymphocytes and some monocytes, while in *Ccr2*–GFP mice, they were monocytes and differentiated macrophages (Extended Data Fig. 5a–

f). We then crossed both $SOD1^{G93A}$ and $SOD1^{G37R}$ mice with either *Ccr2*–GFP or *Ccr2*–RFP mice. Infiltration of $Ccr2^{+}$ cells in ALS mouse spinal cords followed a similar pattern as GFP^{+} cells after busulfan/BM transplantation and confirmed some, but very late, infiltration in slow-progressing $SOD1^{G37R}$ mice, and only very limited, late and transient infiltration in fast-progressing $SOD1^{G93A}$ mice (Extended Data Fig. 5g–k).

Replacing peripheral nerve macrophages with macrophages with less neurotoxic reactive oxygen species responses attenuates both peripheral and central pathology in ALS mice.

On the basis that out of our two ALS models, $SOD1^{G93A}$ mice were the ones showing nearly no peripheral myeloid cell infiltration in the spinal cord, we chose this model to assess disease-modifying capacities of peripheral nerve macrophages (independent of microglia). We used our busulfan/BM grafting strategy to replace peripheral macrophages in $SOD1^{G93A}$ mice at the presymptomatic stage (around 52 days) (Extended Data Figs. 2c and 6a). No differences were measured with respect to sciatic nerve macrophage activation, microglial activation, MN degeneration or lymphocyte infiltration in mice grafted with mutant $SOD1^{G93A}$ BM compared with non-grafted $SOD1^{G93A}$ mice, thereby showing that the BM graft protocol has no impact per se on pathology (Extended Data Figs. 6g and 7a–c).

Replacing $SOD1^{G93A}$-expressing peripheral macrophages with control GFP^{+} macrophages did not show any differences between $GFP \rightarrow SOD1^{G93A}$ and $SOD1^{G93A} \rightarrow SOD1^{G93A}$ mice for nerve macrophage activation, microglial activation, MN degeneration or T lymphocyte infiltration (Fig. 3a,b and Extended Data Fig. 7a–c). Since replacing mutant SOD1-expressing macrophages with control macrophages was not enough to promote neuroprotection, we replaced them with macrophages that were genetically modified to be less neurotoxic or more neurotrophic.

Based on the literature, we selected two candidate genes from a common reactive oxygen species (ROS) pathway with opposite functions. First, *Cybb*, which encodes the (neurotoxic) superoxide-producing Nox2 enzyme (also known as gp91^{phox}), of which full deletion showed robust increased survival in ALS mice[27,28], and second, *Sod1* itself. While this might first appear counterintuitive to use Sod1 in mutant SOD1 mice, the endogenous wild-type Sod1 enzyme detoxifies superoxides produced by Nox2, and Sod1 is neuroprotective in neuronal injury models[29]. Likewise, dismutase-active SOD1 in Schwann cells is protective in ALS mice[6]. Therefore, we thought that downregulating Nox2 or overexpressing Sod1 in peripheral nerve macrophages (but not in microglia or MNs) could be a valuable strategy to beneficially modulate ALS disease in mice.

We replaced (with high efficiency) mutant SOD1-expressing peripheral macrophages with macrophages with reduced neurotoxic ROS responses (Nox2 knockout (KO): Nox2 KO→SOD1^{G93A} or overexpressing wild-type hSOD1^{WT} and GFP: SOD1^{WT}/GFP→SOD1^{G93A}) (Extended Data Figs. 2c and 6a–d). We confirmed for SOD1^{WT}/ GFP→SOD1^{G93A} mice a very low rate of GFP^{+}-infiltrated cells in the spinal cord (Extended Data Fig. 6e,f). MN numbers were unchanged at comparable disease stages or only weakly better for Nox2 KO→SOD1^{G93A} mice at end-stage (Extended Data Fig. 7b), which is possibly linked to the increased numbers of CD4^{+} cells in their spinal cords (Extended Data Fig. 7c–f), which is an effect known to influence MN survival[4,30]. By contrast, in SOD1^{WT}/GFP→SOD1^{G93A} and Nox2 KO→SOD1^{G93A} mice, sciatic nerve macrophage activation was reduced compared with SOD1^{G93A}→SOD1^{G93A} mice (Fig. 3a,c), while macrophage numbers remained constant (Extended Data Fig. 7a). Moreover, CNS microglial activation was significantly reduced in both $SOD1^{WT}$/GFP→$SOD1^{G93A}$ and Nox2 KO→$SOD1^{G93A}$ mice compared with $SOD1^{G93A}$ and $SOD1^{G93A}$→$SOD1^{G93A}$ mice (Fig. 3b,d), which shows that cells at the periphery can modulate microglial activation in the CNS.

By following disease courses of the different grafted mouse groups, the most striking effect was a delayed symptomatic phase, especially in $SOD1^{WT}$/GFP→$SOD1^{G93A}$ mice (Fig. 4a–c and Extended Data Fig. 8). While this was not sufficient to increase survival (Fig. 4c and Extended Data Fig. 8), $SOD1^{WT}$/GFP BM transplantation was able to increase muscle strength (Fig. 4d).

Replacement at disease onset of peripheral nerve macrophages increases survival of ALS mice. As $SOD1^{WT}$/GFP BM transplantation in ALS mice was protective, but only during the early disease phase, we hypothesized that acting later, at disease onset (which would also be clinically more relevant), would affect the later disease phase and survival. Thus, we started busulfan treatment at the mean age of peak weight, at disease onset (at around 102 days; Extended Data Fig. 2c′). This led to a higher proportion of GFP^+ cells in the spinal cord but was variable among mice. There was no correlation between the proportion of infiltrated monocytes/macrophages and survival of disease-onset-grafted $SOD1^{WT}$/GFP→$SOD1^{G93A}$ mice, which indicates that higher infiltration does not influence disease progression (Fig. 5a–c). Engraftment of $CD11b^+$ cells into the blood was efficient (63.7 ± 3.2% at day 12 and 91.2 ± 3.2% at day 24 after grafting, n = 17), while peripheral macrophage replacement in the sciatic nerve was lower than in mice grafted at the presymptomatic stage (Fig. 5d and Extended Data Fig. 6d). Other peripheral macrophages in unaffected tissues, such as lymph nodes, were, however, not replaced (4.51 ± 0.45% GFP^+ macrophages, $n = 3$ onset-grafted $SOD1^{WT}$/GFP→$SOD1^{G93A}$ mice).

MN and $CD3^+$ cell numbers (at similar disease stages) were not different in the two groups of onset-grafted mice (Fig. 5e,f). Among $CD3^+$ cells, while $Foxp3^+$ neuroprotective regulatory T lymphocyte (T_{reg}) cell numbers were modified during disease in $SOD1^{G93A}$ mice, as previously described[31], no difference was measured between onset-grafted $SOD1^{WT}$/GFP→$SOD1^{G93A}$ and $SOD1^{G93A}$→$SOD1^{G93A}$ mice (Fig. 5g and Extended Data Fig. 7g). Grafting $SOD1^{G93A}$ mice at disease onset with $SOD1^{WT}$/GFP BM also led to reduced sciatic nerve macrophage activation (Fig. 5h) compared with $SOD1^{G93A}$→$SOD1^{G93A}$ mice, while, as before, macrophage numbers remained constant (Fig. 5i). Importantly, we again observed decreased spinal cord microglial activation (Fig. 5j).

$SOD1^{G93A}$ mice grafted at disease onset with $SOD1^{WT}$/GFP BM reached the symptomatic stage later and showed increased survival compared with onset-grafted $SOD1^{G93A}$→$SOD1^{G93A}$ mice (Fig. 5k,l). Control experiments of grafting $SOD1^{G93A}$ mice with $SOD1^{G93A}$ BM at disease onset did not change any disease parameters, thereby showing no impact of the graft per se on pathology (Extended Data Fig. 8b′,c). Therefore, the timing of peripheral macrophage replacement is a crucial parameter for macrophage modulation, and it is possible to slow disease progression and increase ALS mouse survival by modifying macrophages at the periphery.

RNA sequencing analysis identifies the sciatic nerve peripheral macrophage response over the disease course in ALS mice and reveals profound differences with the

reaction profile of spinal cord microglia. Since improvements in ALS mouse survival depended on the timing of grafting and since presymptomatic grafting slowed disease progression until the symptomatic phase but did not affect the end-stage, we hypothesized that macrophage reactivity profiles would strongly change over the course of the disease. We therefore analyzed the sciatic nerve peripheral macrophage transcriptome by RNA sequencing (RNA-seq) throughout disease progression (Extended Data Fig. 9a, Supplementary Fig. 2a and Supplementary Tables 2 and 3). Since modifying peripheral macrophages influenced microglial activation, we also analyzed the spinal cord microglia transcriptome at the same disease stages (presymptomatic, onset, early symptomatic and end-stage) in SOD1^{G93A} and control mice (Extended Data Fig. 9a, Supplementary Fig. 2a and Supplementary Tables 2 and 4). Our protocol avoided enzymatic treatment to minimize extrinsic cell activation (Supplementary Fig. 2a). We confirmed the viability and purity of our CD11b^{+} cells; all were F4/80^{+} monocytes/macrophages, but not Sox10^{+} Schwann cells or elastase^{+} neutrophils (Supplementary Fig. 2b–w).

On average, there were 18,171 expressed genes in microglia and 14,080 in peripheral nerve macrophages. Although macrophages and microglia shared the majority of their expressed genes, thus confirming their common myeloid identity, both cell types expressed specific genes (Extended Data Fig. 9b). We used literature based microglial-specific and macrophage-specific genes and showed that their expression in our RNA-seq data could discriminate the two populations (Extended Data Fig. 10), which is in line with recent transcriptomic data from nerve macrophages[26]. Siglec-1 was not specific, thereby confirming our immunostaining data (Extended Data Figs. 4 and 10).

The most striking finding was the clear segregation in the principal component analysis (PCA) between peripheral nerve macrophages and microglia rather than between the four disease stages (Fig. 6a). This showed that the two cell populations reacted differently to the disease and, importantly, stayed different even through the activation process. We then analyzed differences between time points and cell types (Extended Data Fig. 9c and Supplementary Table 5). Heatmap analyses of genes regulated by nerve macrophages revealed that regulation profiles were not progressive but abruptly changed. There were modifications among each of the four time points analyzed, including between onset and early symptomatic and early symptomatic and end-stage (Fig. 6b). The microglial gene regulation profiles were more unidirectional (mostly upregulated from presymptomatic onwards) and progressive (Fig. 6b). Thus, gene regulation patterns are extremely different between macrophages and microglia.

To more precisely visualize the gene regulation patterns, clustering of gene expression profiles was performed according to their evolution throughout the disease stages. While only five different clusters of gene expression profiles were detectable in microglia, peripheral nerve macrophages showed 18 profiles, further highlighting the differences in reactive responses between the two cell populations (Fig. 6c). This showed again that macrophage gene regulation profiles changed their orientation between onset and early-symptomatic stage and between early symptomatic and end-stage (Fig. 6b,c).

To assess the functional differences between the reaction profiles of macrophages and microglia, we identified the top regulated pathways (via Kyoto Encyclopedia of Genes and Genomes (KEGG) analysis) corresponding to each of the different clusters of expression profiles. This revealed two groups of pathways that were specifically regulated either in macrophages or microglia. A third group overlapped between macrophages and microglia (with some pathways linked to inflammation); however, regulation patterns were completely different, with macrophages exhibiting abrupt temporal changes while microglia exhibited progressive, unidirectional changes (Fig. 6d).

We focused on nerve macrophage responses using a more specific Gene Ontology (GO) term analysis. We identified the top five 'biological process' GO terms from comparisons between consecutive disease stages and additional regulated GO terms related to 'immune function' and 'cell proliferation' (Fig. 6e). Most of these pathways (18 out of 21) were only regulated at specific disease stages, thereby revealing different response phases. The top regulated GO terms at the beginning of the disease (presymptomatic to onset) were related to 'protein transport', 'gene expression' and 'signal transduction', which could represent early reactions of macrophages to the nerve affection. Between onset and the early-symptomatic stage, regulated genes were related to cellular responses to stress (GO terms 'cellular response to DNA damage stimulus' and 'DNA repair'), which could be linked to increased oxidative stress during macrophage activation (that is, increasing the risk of DNA damage[32]). At this stage, many genes implicated in cell proliferation were regulated, which correlated with the increased sciatic nerve macrophage numbers we measured (Fig. 1f). In the fully symptomatic phase (early symptomatic to end-stage), GO terms related to 'immunity' and 'inflammation' were regulated, thereby supporting neuroinflammatory processes as being especially implicated in disease progression (Fig. 6e). To assess the influence of these pathways in more detail, we asked whether and how they were changed by our initial functional approach of modifying peripheral macrophages to increase survival.

The survival-promoting effect of grafting modified macrophages is linked to a shift in macrophage inflammatory reactivity and an inversion of microglial responses toward neuronal support. We extracted sciatic nerve macrophages and microglia from onset-grafted $SOD1^{WT}{\rightarrow}SOD1^{G93A}$ mice (which survived longer) and from $SOD1^{G93A}{\rightarrow}SOD1^{G93A}$ mice at the early-symptomatic stage and end-stage and performed RNA-seq (Extended Data Fig. 9a and Supplementary Table 6). Comparison analyses of macrophages between SOD1^{WT}→SOD1^{G93A} and SOD1^{G93A}→SOD1^{G93A} mice showed that at the early-symptomatic stage, the effect of the modified, protective (SOD1^{WT}→SOD1^{G93A}) graft led to a strong downregulation of a large group of genes (1,090 downregulated, 283 upregulated) that was sustained until the end-stage (Fig. 7a,b and Extended Data Fig. 9c). However, the effect of the modified peripheral macrophage graft on microglia was very different, with most of the regulated genes upregulated (1,642 upregulated and 65 downregulated), but not maintained, with only 134 regulated genes at the end-stage (Fig. 7c and Extended Data Fig. 9c).

In macrophages, at the early-symptomatic stage, ingenuity pathway analysis (IPA) showed a close to complete inversion of inflammatory pathways related to immune cell trafficking by the SOD1^{WT}→SOD1^{G93A} graft, thereby downregulating this inflammation (Fig. 7a). This inversion by the SOD1^{WT}→SOD1^{G93A} graft was also visible on a broader level on different pathways regulated over the course of disease (between presymptomatic and early symptomatic) in SOD1^{G93A} macrophages (Fig. 7b, the top 25 pathways are shown).

Theswitchinmacrophageactivationafterthe SOD1^{WT}→SOD1^{G93A} graft was accompanied by changes in microglial responses (Fig. 7c). Activation of inflammatory pathways throughout the disease course in SOD1^{G93A} microglia was reduced by the graft (Fig. 7c), which is consistent with the microglial activation downregulation measured by Iba1 immunostaining (Fig. 5j). Downregulated inflammatory genes included *Il1b*, *S100a8* (involved in the Toll-like receptor pathway), *Arpc2* (involved in macrophage integrin phagocytosis function), *Ccr1*, while upregulated anti-inflammatory or (neuro)trophic genes included *Vegfa*, *Cntfr*, *Fgf1* and *Fgfr3* (Supplementary Table 6). Remarkably, pathways downregulated in microglia throughout the disease course were globally inversed and upregulated by the $SOD1^{WT}$→$SOD1^{G93A}$ graft at the early-symptomatic stage (Fig. 7c). The two most significant pathways were 'oxidative phosphorylation' and 'synaptogenesis signaling pathway'. A comparison of regulated genes over the disease course (presymptomatic to end-stage) in $SOD1^{G93A}$ microglia with those from $SOD1^{WT}$→$SOD1^{G93A}$ (compared with $SOD1^{G93A}$→$SOD1^{G93A}$) microglia at the early-symptomatic stage showed a complete inversion of the regulation of more than 1,000 genes (with most, 1,030 genes, switching from downregulation to upregulation, and 19 from upregulation to downregulation) (Fig. 7d). Among these genes were 120 related to 'synapse' GO or IPA terms, including 39 genes from the IPA 'synaptogenesis signaling pathway', which were all upregulated by the $SOD1^{WT}$→ $SOD1^{G93A}$ graft (Fig. 7d). Fifty genes of the IPA 'synaptogenesis signaling pathway' were upregulated (and two downregulated) in $SOD1^{WT}$→$SOD1^{G93A}$ microglia (compared with $SOD1^{G93A}$→ $SOD1^{G93A}$) at the early-symptomatic stage (Fig. 7c). By contrast, from the same pathway, 95 genes were downregulated (and 33 upregulated) in microglia of $SOD1^{G93A}$ mice throughout the disease course (presymptomatic to end-stage) (Fig. 7c). The graft led to the inversion of 39 genes (from downregulation to upregulation) in favor of increased synaptic/neuronal support at the early-symptomatic stage in $SOD1^{WT}$→$SOD1^{G93A}$ microglia (Fig. 7d).

Discussion

By focusing on the MN peripheral compartment, we identified a novel target to modulate ALS disease: peripheral nerve macrophages. By directly comparing sciatic nerve peripheral macrophages to CNS microglia, we generated a unique longitudinal transcriptomic dataset of how the macrophages in the two compartments of MNs react to neurodegeneration in ALS.

Replacing peripheral macrophages at disease onset extended survival and decreased peripheral macrophage inflammation and inverted microglial responses triggered by ALS. Our study provides an answer to the long-standing debate of whether peripheral monocytes/macrophages infiltrate the CNS during ALS. While previous studies suggested strong infiltration, they mostly used irradiation-based methods[10,16–18], inducing artifact cell infiltration[19,20]. We cannot rule out that busulfan on its own could have an impact on ALS mice that is exacerbated with the disease, as conditions such as stress are known to increase cell infiltration[33]. However, we chose a dose range that shows no impact on the CNS[34], and our $SOD1^{G93A}$→$SOD1^{G93A}$ mice were similar to non-grafted $SOD1^{G93A}$ mice. We showed that CNS infiltration of peripheral myeloid cells depended on disease progression and was low in fast-progressing $SOD1^{G93A}$ mice. Since the amount of infiltrated myeloid cells results from infiltration and local proliferation[17,35], the extended disease course in $SOD1^{G37R}$ mice could have led to an accumulation of infiltrated cells through proliferation rather than infiltration.

An unresolved but crucial question is whether the two myeloid cell types surrounding MNs react the same to the disease. To answer this, we used disease-relevant peripheral macrophages from the sciatic nerve. By contrast, previous transcriptomic analyses used data-bases (Immunologival Genome Project (ImmGen) consortium) of different types of monocytes/macrophages, and not from ALS mice or in contact with degenerating MNs[22]. Our study demonstrated that during disease, spinal cord microglia around MN soma and peripheral nerve macrophages around motor axons react very differently to ongoing MN degeneration. Both the different ontogenies of microglia and macrophages and/or inherent differences of the two environments they react in could have contributed to their unique reaction profiles. This underlines that microglia and peripheral nerve macrophages represent two separate entities to modulate the innate immune system during neurodegeneration.

The impact of peripheral monocytes/macrophages on ALS has so far been mainly considered after infiltration of peripheral cells into the affected CNS. Studies came to opposite conclusions, with infiltrating monocytes/macrophages being either detrimental or protective[21,25]. Similarly, in studies using irradiation, which recruited control myeloid cells into the CNS of ALS mice, discordant conclusions showed either positive or no effects on disease duration[10,16]. The effects of monocyte/macrophage at the periphery were considered by comparing the timing of activation of nerve macrophages and microglia, but this was assessed using a CSF1R inhibitor that targets both peripheral macrophages and microglia[9,36]. These studies concluded that nerve macrophages were affected before microglia and that participation of peripheral macrophages to the disease was likely. In addition, differences in blood monocyte transcriptomes of patients with ALS compared with controls have been reported[25,37]. However, modulating disease by targeting peripheral macrophages, independent of microglia, had previously not been achieved. Since the proportion of Iba1^{+} cells originating from the periphery in the spinal cord of onset-grafted SOD1^{WT}/ GFP→SOD1^{G93A} mice did not correlate with mouse survival, the protection we obtained with modified BM transplantation came from the periphery.

BM grafting affects the generation of all BM-derived cell types. CD4^{+} lymphocytes are protective in ALS independent of their expression of mutant SOD1 (refs. [4,30]). CD8^{+} lymphocytes are deleterious for MNs and for ALS mouse survival[38,39]. However, the contribution to ALS mouse survival of mutant SOD1 expressed by CD8^{+} cells remains undetermined. While increased infiltration of CD3^{+} and especially T_{reg} (Foxp3^{+}) cells into the CNS modulates ALS mouse survival and is predictive of ALS disease progression[31,40], we found no difference in the number of infiltrated T_{reg} cells in response to neuroprotective BM (SOD1^{WT}→SOD1^{G93A}) engraftment, which suggests that there is no contribution of T cell replacement in our specific SOD1^{WT}/GFP→SOD1^{G93A} grafting situation.

Removing B lymphocytes has no effect, while altering the number of infiltrated natural killer cells affects ALS mouse survival, but only if done presymptomatically[41–43]. Mast cells and neutrophils were reported in nerves of symptomatic SOD1^{G93A} rats and in nerves and muscles of patients with ALS, and blocking mast cells with masitinib was beneficial in rats[44]. However, since masitinib also targets CSF1R, which is expressed by macrophages and microglia, this positive effect could partly be due to a reduction in the activation of other myeloid cells[44–47]. To our knowledge, the role of granulocytes has not been studied in ALS. Our BM grafting resulted in the replacement of sciatic nerve macrophages, whereas other peripheral phagocytes, such as lymph node macrophages, were not replaced. Thus, although we cannot exclude potential effects of other BM-derived cell types, the major part of the neuroprotective effect can be attributed to BM-derived nerve macrophages localized close to the affected MN axons.

The beneficial impact of modified BM cells on disease progression in SOD1^{G93A} mice seemed linked to their capacity to modify both peripheral nerve macrophages and CNS microglial reactivity. Replacing peripheral nerve macrophages could result in the MNs being less affected and in turn less prone to activate surrounding microglia. Increased survival was only obtained when mice were transplanted at disease onset, which shows that the timing of macrophage replacement is essential and suggests that the trophic capacities of peripheral macrophages are lost over time. However, gene regulation changes in onset-grafted macrophages were maintained from early symptomatic to end-stage, but not in microglia, where they faded. Increased survival could be linked to a direct effect of peripheral macrophages on MN axons or indirectly on MN soma through microglia; however, both linked to an effect originating from the periphery. Acting at the periphery led to modulation of the 'synaptogenesis signaling' pathway toward a beneficial synaptic/neuronal support profile by microglia. These synaptic genes were previously reported as expressed by microglia (70% with datasets from Brain RNA-Seq (http://brainrnaseq.org) and ImmGen.org (http:// www.immgen.org)) and were found to be regulated (57% of our list) in a previous study of the microglial transcriptome in SOD1^{G93A} mice[22]. Thirty percent of our synaptic gene list overlapped with microglial genes implicated in 'nervous system development and function' during development[48]. Microglia express neurotransmitter receptors and play a crucial role in pruning and synaptic stripping during development and injury[49,50]. We showed that modulating macrophages at the periphery during the progressive neurodegenerative disease phase of ALS can reduce pathological proinflammatory microglial responses and reverse their disease-related downregulation of genes linked to synaptic/neuronal support.

In conclusion, modifying peripheral macrophages can downregulate inflammation at the periphery along nerves and in the CNS, and peripheral macrophages can influence disease progression and ALS mouse survival, with the timing of intervention being crucial. Since BM transplantation is reported as safe procedure in patients with ALS[5], our study provides proof of principle that modulating cells (macrophages) at the periphery (along nerves) could be of therapeutic value in ALS.

References

1. Rosen, D. R. *et al.* Mutations in Cu/Zn superoxide dismutase gene are associated with familial amyotrophic Lateral Sclerosis. *Nature* **362**, 59–62 (1993).

2. Gurney, M. E. *et al.* Motor neuron degeneration in mice that express a human Cu,Zn superoxide dismutase mutation. *Science* **264**, 1772–1775 (1994).

3. Boillée, S. *et al.* Onset and progression in inherited ALS determined by motor neurons and microglia. *Science* **312**, 1389–1392 (2006).

4. Beers, D. R., Henkel, J. S., Zhao, W., Wang, J. & Appel, S. H. CD4+ T cells support glial neuroprotection, slow disease progression, and modify glial morphology in an animal model of inherited ALS. *Proc. Natl. Acad. Sci. U. S. A.* **105**, 15558–15563 (2008).

5. Appel, S. H. *et al.* Hematopoietic stem cell transplantation in patients with sporadic amyotrophic lateral sclerosis. *Neurology* **11**, 1326–1334 (2008).

6. Lobsiger, C. S. *et al.* Schwann cells expressing dismutase active mutant SOD1 unexpectedly slow disease progression in ALS mice. *Proc. Natl. Acad. Sci. U. S. A.* **106**, 4465–4470 (2009).

7. Beers, D. R. *et al.* Wild-type microglia extend survival in PU . 1 knockout mice with familial amyotrophic lateral sclerosis. *Proc. Natl. Acad. Sci.* **103**, 16021–16026 (2006).

8. Wang, L., Sharma, K., Grisotti, G. & Roos, R. P. The effect of mutant SOD1 dismutase activity on non-cell autonomous degeneration in familial amyotrophic lateral sclerosis. *Neurobiol. Dis.* **35**, 234–240 (2009).

9. Martínez-Muriana, A. *et al.* CSF1R blockade slows the progression of amyotrophic lateral sclerosis by reducing microgliosis and invasion of macrophages into peripheral nerves. *Sci. Rep.* **6**, 1–13 (2016).

10. Chiu, I. M. *et al.* Activation of innate and humoral immunity in the peripheral nervous system of ALS transgenic mice. *Proc. Natl. Acad. Sci. U. S. A.* **106**, 20960–20965 (2009).

11. Lincecum, J. M. *et al.* From transcriptome analysis to therapeutic anti-CD40L

treatment in the SOD1 model of amyotrophic lateral sclerosis. *Nat. Genet.* **42**, 392–399 (2010).

12. Fischer, L. R. *et al.* Amyotrophic lateral sclerosis is a distal axonopathy: evidence in mice and man. *Exp. Neurol.* **185**, 232–240 (2004).
13. Ginhoux, F. *et al.* Fate Mapping Analysis Reveals That Adult Microglia Derive from Primitive Macrophages. *Science.* **330**, 841–845 (2010).
14. Gosselin, D. *et al.* Environment drives selection and function of enhancers controlling tissue-specific macrophage identities. *Cell* **159**, 1327–1340 (2014).
15. Lavin, Y. *et al.* Tissue-resident macrophage enhancer landscapes are shaped by the local microenvironment. *Cell* **159**, 1312–1326 (2014).
16. Corti, S. *et al.* Wild-type bone marrow cells ameliorate the phenotype of SOD1-G93A ALS mice and contribute to CNS, heart and skeletal muscle tissues. *Brain* **127**, 2518–32 (2004).
17. Solomon, J. N. *et al.* Origin and distribution of bone marrow-derived cells in the central nervous system in a mouse model of amyotrophic lateral sclerosis. *Glia* **53**, 744–753 (2006).
18. Lewis, C.-A. B., Solomon, J. N., Rossi, F. M. & Krieger, C. Bone marrow-derived cells in the central nervous system of a mouse model of amyotrophic lateral sclerosis are associated with blood vessels and express CX(3)CR1. *Glia* **57**, 1410–9 (2009).
19. Ajami, B., Bennett, J. L., Krieger, C., Tetzlaff, W. & Rossi, F. M. V. Local self-renewal can sustain CNS microglia maintenance and function throughout adult life. *Nat. Neurosci.* **10**, 1538–1543 (2007).
20. Mildner, A. *et al.* Microglia in the adult brain arise from Ly-6ChiCCR2+ monocytes only under defined host conditions. *Nat. Neurosci.* **10**, 1544–1553 (2007).
21. Butovsky, O. *et al.* Modulating inflammatory monocytes with a unique microRNA

gene signature ameliorates murine ALS. *J. Clin. Invest.* **122**, 3063–3087 (2012).

22. Chiu, I. M. *et al.* A neurodegeneration-specific gene-expression signature of acutely isolated microglia from an amyotrophic lateral sclerosis mouse model. *Cell Rep.* **4**, 385–401 (2013).

23. Bennett, F. C. *et al.* A Combination of Ontogeny and CNS Environment Establishes Microglial Identity. *Neuron* **98**, 1170-1183.e8 (2018).

24. Bennett, M. L. *et al.* New tools for studying microglia in the mouse and human CNS. *Proc. Natl. Acad. Sci.* **12**, E1738–E1746 (2016).

25. Zondler, L. *et al.* Peripheral monocytes are functionally altered and invade the CNS in ALS patients. *Acta Neuropathol.* **132**, 391–411 (2016).

26. Ydens, E. *et al.* Profiling peripheral nerve macrophages reveals two macrophage subsets with distinct localization, transcriptome and response to injury. *Nat. Neurosci.* **5**, 676–689 (2020).

27. Marden, J. J. *et al.* Redox modifier genes in amyotrophic lateral sclerosis in mice. *J. Clin. Invest.* **117**, 2913–2919 (2007).

28. Wu, D.-C., Ré, D. B., Nagai, M., Ischiropoulos, H. & Przedborski, S. The inflammatory NADPH oxidase enzyme modulates motor neuron degeneration in amyotrophic lateral sclerosis mice. *Proc. Natl. Acad. Sci. U. S. A.* **103**, 12132–12137 (2006).

29. Sugawara, T., Lewén, A., Gasche, Y., Yu, F. & Chan, P. H. Overexpression of SOD1 protects vulnerable motor neurons after spinal cord injury by attenuating mitochondrial cytochrome c release. *FASEB J.* **16**, 1997–1999 (2002).

30. Chiu, I. M. *et al.* T lymphocytes potentiate endogenous neuroprotective inflammation in a mouse model of ALS. *Proc. Natl. Acad. Sci. U. S. A.* **105**, 17913–17918 (2008).

31. Beers, D. R. *et al.* Endogenous regulatory T lymphocytes ameliorate amyotrophic

lateral sclerosis in mice and correlate with disease progression in patients with amyotrophic lateral sclerosis. *Brain* **134**, 1293–314 (2011).

32. Virág, L., Jaén, R. I., Regdon, Z., Boscá, L. & Prieto, P. Self-defense of macrophages against oxidative injury: Fighting for their own survival. *Redox Biol.* **26** (2019).

33. Ataka, K. *et al.* Bone marrow-derived microglia infiltrate into the paraventricular nucleus of chronic psychological stress-loaded mice. *PLoS One* **8**, 1–14 (2013).

34. Kierdorf, K., Katzmarski, N., Haas, C. a. & Prinz, M. Bone Marrow Cell Recruitment to the Brain in the Absence of Irradiation or Parabiosis Bias. *PLoS One* **8**, 1–10 (2013).

35. Peake, K. *et al.* Bone Marrow-Derived Cell Accumulation in the Spinal Cord Is Independent of Peripheral Mobilization in a Mouse Model of Amyotrophic Lateral Sclerosis. *Front. Neurol.* **8**, 1–13 (2017).

36. Nardo, G. *et al.* Immune response in peripheral axons delays disease progression in SOD1 G93A mice. *J. Neuroinflammation* **13**, 1–16 (2016).

37. Zhao, W. *et al.* Characterization of gene expression phenotype in amyotrophic lateral sclerosis monocytes. *JAMA Neurol.* **74**, 677–685 (2017).

38. Nardo, G. *et al.* Counteracting roles of MHCI and CD8 + T cells in the peripheral and central nervous system of ALS SOD1 G93A mice. *Mol. Neurodegener.* **13**, 1–24 (2018).

39. Coque, E. *et al.* Cytotoxic CD8 + T lymphocytes expressing ALS-causing SOD1 mutant selectively trigger death of spinal motoneurons. *PNAS* **6**, 2312–2317 (2019).

40. Henkel, J. S. *et al.* Regulatory T-lymphocytes mediate amyotrophic lateral sclerosis progression and survival. *EMBO Mol. Med.* **5**, 64–79 (2013).

41. Komine, O. *et al.* Innate immune adaptor TRIF deficiency accelerates disease progression of ALS mice with accumulation of aberrantly activated astrocytes. *Cell Death Differ.* **25**, 1–17 (2018).

42. Naor, S. *et al.* Development of ALS-like disease in SOD-1 mice deficient of B lymphocytes. *J. Neurol.* **256**, 1228–1235 (2009).

43. Garofalo, S. *et al.* Natural killer cells modulate motor neuron-immune cell cross talk in models of Amyotrophic Lateral Sclerosis. *Nat. Commun.* **11,** 1173 (2020)

44. Trias, E. *et al.* Mast cells and neutrophils mediate peripheral motor pathway degeneration in ALS Graphical abstract Find the latest version : Mast cells and neutrophils mediate peripheral motor pathway degeneration in ALS. *J. Clin. Investig. Insight* **3**, e123249 (2018).

45. Trias, E. *et al.* Evidence for mast cells contributing to neuromuscular pathology in an inherited model of ALS. *JCI Insight* **2**, 1–14 (2017).

46. Graves, M. C. *et al.* Inflammation in amyotrophic lateral sclerosis spinal cord and brain is mediated by activated macrophages , mast cells and T cells. *ALS other Mot. neuron Disord.* **5**, 213–219 (2004).

47. Staats, K. A. *et al.* C-kit is important for $SOD1^{G93A}$ mouse survival independent of mast cells. *Neuroscience* **301**, 415–420 (2015).

48. Thion, M. S. *et al.* Microbiome Influences Prenatal and Adult Microglia in a Sex-Specific Manner. *Cell* **172**, 500–516 (2018).

49. Pocock, J. M. & Kettenmann, H. Neurotransmitter receptors on microglia. *Trends Neurosci.* **30**, 527–535 (2007).

50. Hong, S., Dissing-Olesen, L. & Stevens, B. New insights on the role of microglia in synaptic pruning in health and disease Soyon. *Curr. Opin. Neurobiol.* **36**, 128–134 (2016).

FIGURES

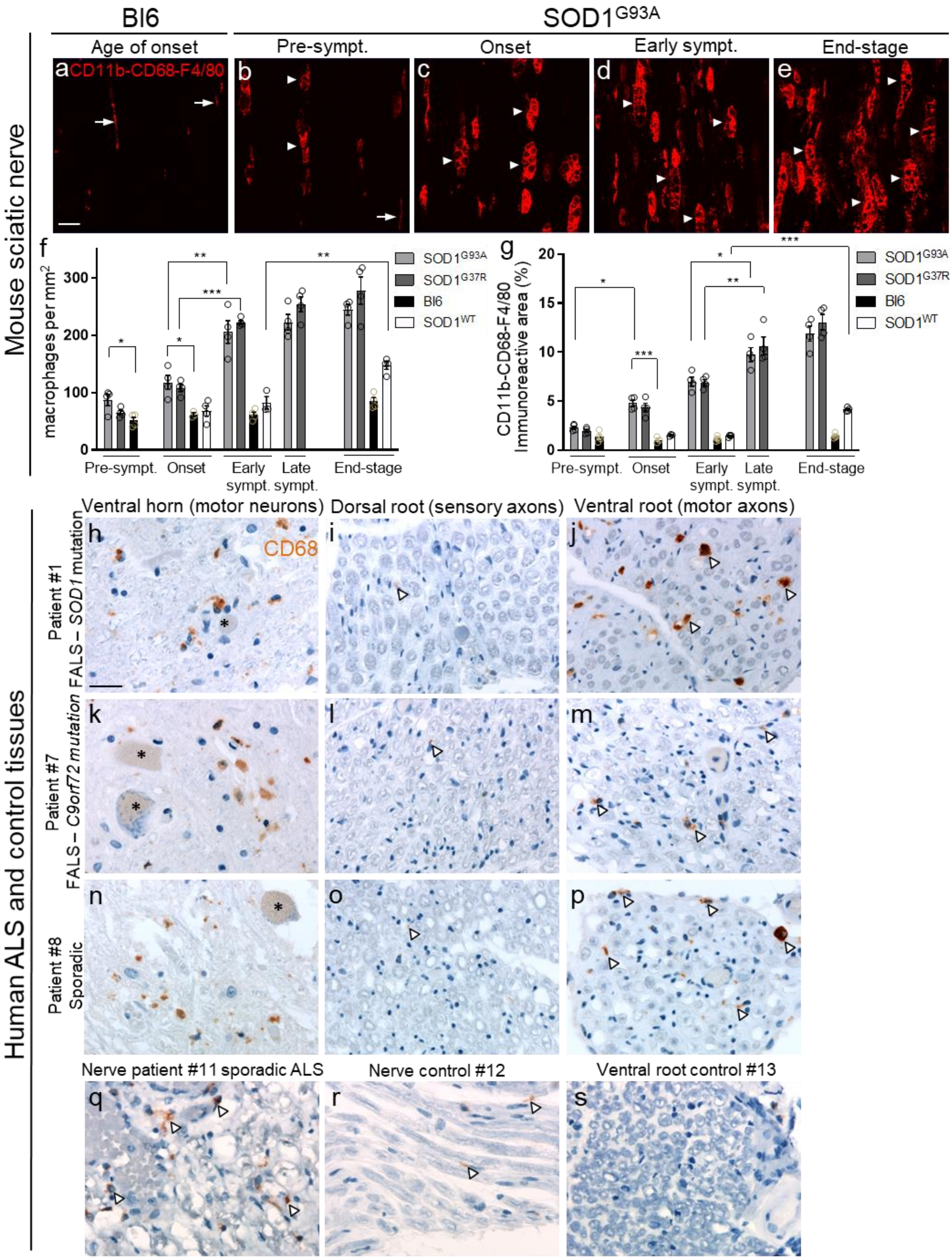

Chiot et al. Figure 1

Fig. 1 | Peripheral nerve macrophages are activated over the course of disease in fast-progression SOD1^{G93A} and slow-progression SOD1^{G37R} ALS mice and in patients with ALS. a–**e**, Immunostaining of sciatic nerves for the macrophage markers CD11b, CD68 and F4/80 in 100-day-old control C57Bl6 (Bl6) (**a**) and SOD1^{G93A} (**b**–**e**) mice at different disease stages: presymptomatic (Presympt.) (**b**), onset (**c**), early symptomatic (Early sympt.) (**d**) and end-stage (**e**). Arrowheads indicate enlarged macrophages, while arrows indicate thin macrophages. Scale bar, 100 μm. **f**,**g**, Quantification of CD11b^{+}CD68^{+}F4/80^{+} macrophages by cell density (**f**) and activation measured by the CD11b-CD68-F4/80-immunoreactive area (**g**) in SOD1^{G93A} (*n* = 4 mice), SOD1^{G37R} (*n* = 4 mice), Bl6 (*n* = 4 or *n* = 3 mice for onset) and SOD1^{WT} (*n* = 4 or *n* = 3 mice for early symptomatic) sciatic nerves. The mean ages ± s.e.m. reached at the different disease stages were, respectively, for SOD1^{G93A} and SOD1^{G37R}: presymptomatic: 52.5 ± 1.3 days and 142 ± 2.3 days; onset (peak weight): 105.3 ± 1.3 days and 240.3 ± 10.7 days; early symptomatic (10% of weight loss): 149.5 ± 3.8 days and 362 ± 5.7 days; late symptomatic (late sympt.; 15% of weight loss): 159.5 ± 4.3 days and 393 ± 16 days; and end-stage (full paralysis): 171.8 ± 4.6 days and 421.25 ± 11.3 days. Bl6 and SOD1^{WT} mice were age-matched to SOD1^{G93A} mice. Data are shown as the mean ± s.e.m.; **P* < 0.05, ***P* < 0.01, ****P* < 0.001, one-way ANOVA followed by a Tukey's post hoc analysisof mean differences. **h**–**s**, Immunostaining against the microglia/macrophage marker CD68 of human ALS spinal cord ventral horn (**h**,**k**,**n**), dorsal root (containing sensory neuron axons) (**i**,**l**,**o**), ventral roots (containing MN axons) (**j**,**m**,**p**), human ALS peripheral nerve (**q**), control peripheral nerve (**r**) and control ventral root (**s**) sections. Arrowheads indicate activated macrophages, while asterisks indicate MN cell bodies. Scale bars, 40 μm. Data associated with the 11 patients with ALS and 4 controls are provided in Supplementary Table 1.

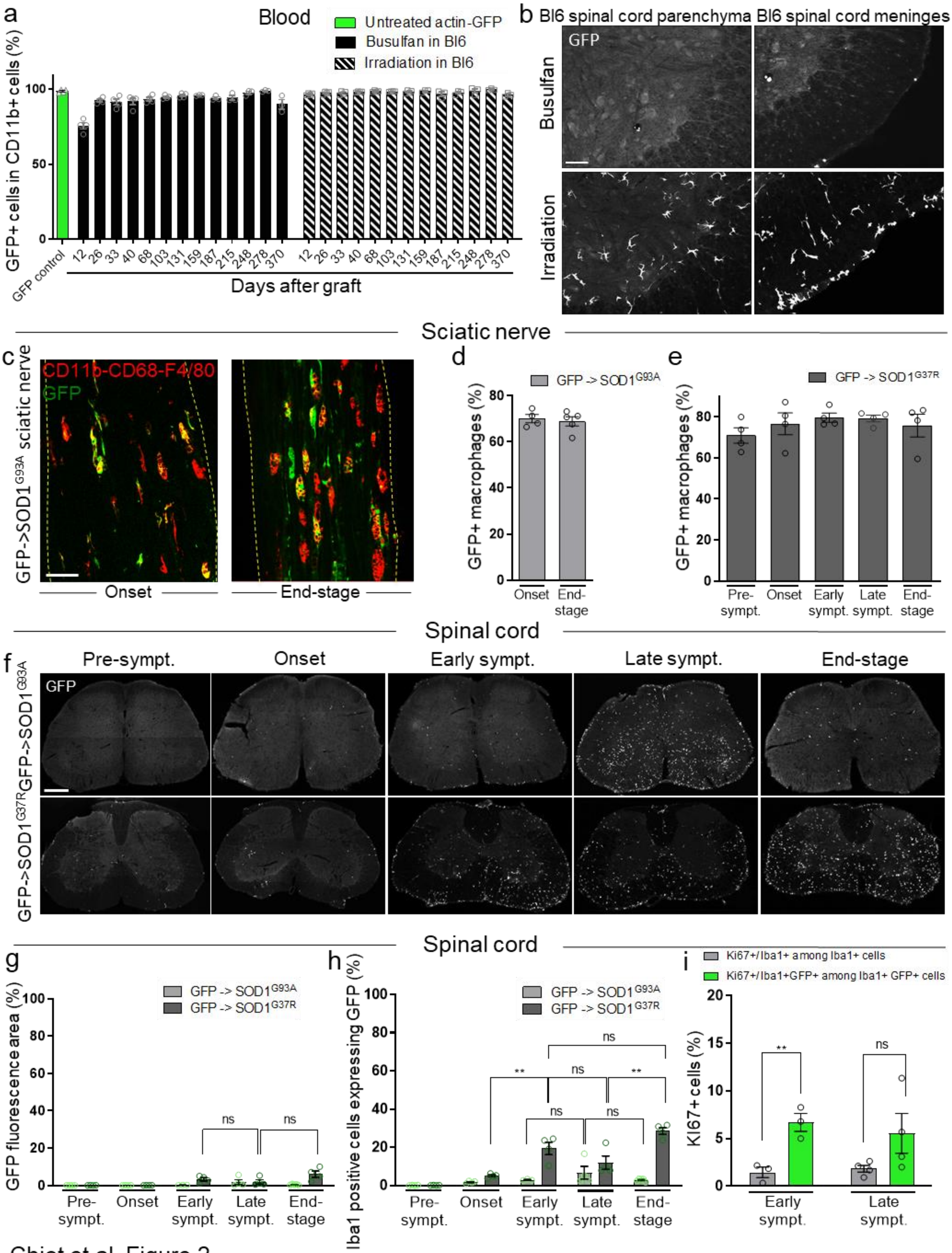

Chiot et al. Figure 2

Fig. 2 | Infiltration of peripheral myeloid cells into the spinal cord of mutant SOD1-expressing ALS mice is weak and depends on the rate of disease progression. a, The proportion of GFP^{+} cells in blood CD11b^{+} myeloid cells of actin–GFP (green) or C57Bl6 (Bl6) mice transplanted with actin–GFP BM after myeloablation with busulfan or irradiation (*n* = 3 or 4 mice). **b**, Spinal cord sections of busulfan-treated or irradiated mice 1 year after transplantation showing GFP^{+} cells originating from the periphery (*n* = 4 mice). **c**, Sciatic nerves of busulfan-treated, actin–GFP-BM-grafted SOD1^{G93A} mice (GFP→SOD1^{G93A}) immunostained for the macrophage markers CD11b, CD68 and F4/80 (red) and showing GFP^{+} cells (green). **d**,**e**, The proportion of GFP^{+} macrophages among all CD11b^{+}CD68^{+}F4/80^{+} macrophages in sciatic nerves of GFP→SOD1^{G93A} (**d**) or GFP→SOD1^{G37R} (**e**) mice (grafted presymptomatically at the mean ages of 52 and 87 days, respectively). *n* = 4 (onset), *n* = 5 (end-stage) mice for GFP→SOD1^{G93A}, and *n* = 4 mice for GFP→SOD1^{G37R} mice. **f**, Images of lumbar spinal cords of GFP→SOD1^{G93A} and GFP→SOD1^{G37R} mice showing GFP^{+} cells originating from the periphery (*n* = 3–5 mice per group). **g**,**h**, The area occupied by GFP fluorescence (**g**) and the number of GFP^{+} cells originating from the periphery in ALS mouse spinal cords as a proportion of Iba^{+} cells expressing GFP (**h**) (*n* = 3–5 mice). **i**, GFP^{+} (green) or GFP^{-} (gray) proliferating (Ki67^{+}) Iba1^{+} cells in GFP→SOD1^{G93A} mouse spinal cords (*n* = 3–4 mice). For **a**,**d**,**e** and **g**–**i**, data are shown as the mean ± s.e.m. $^{**}P < 0.01$, NS, not significant, determined by one-way ANOVA followed by Tukey's post hoc analysis of mean differences (**g** and **h**) or two-tailed Student's *t*-test (**i**). Scale bars, 50 µm (**b** and **c**) or 100 µm (**f**).

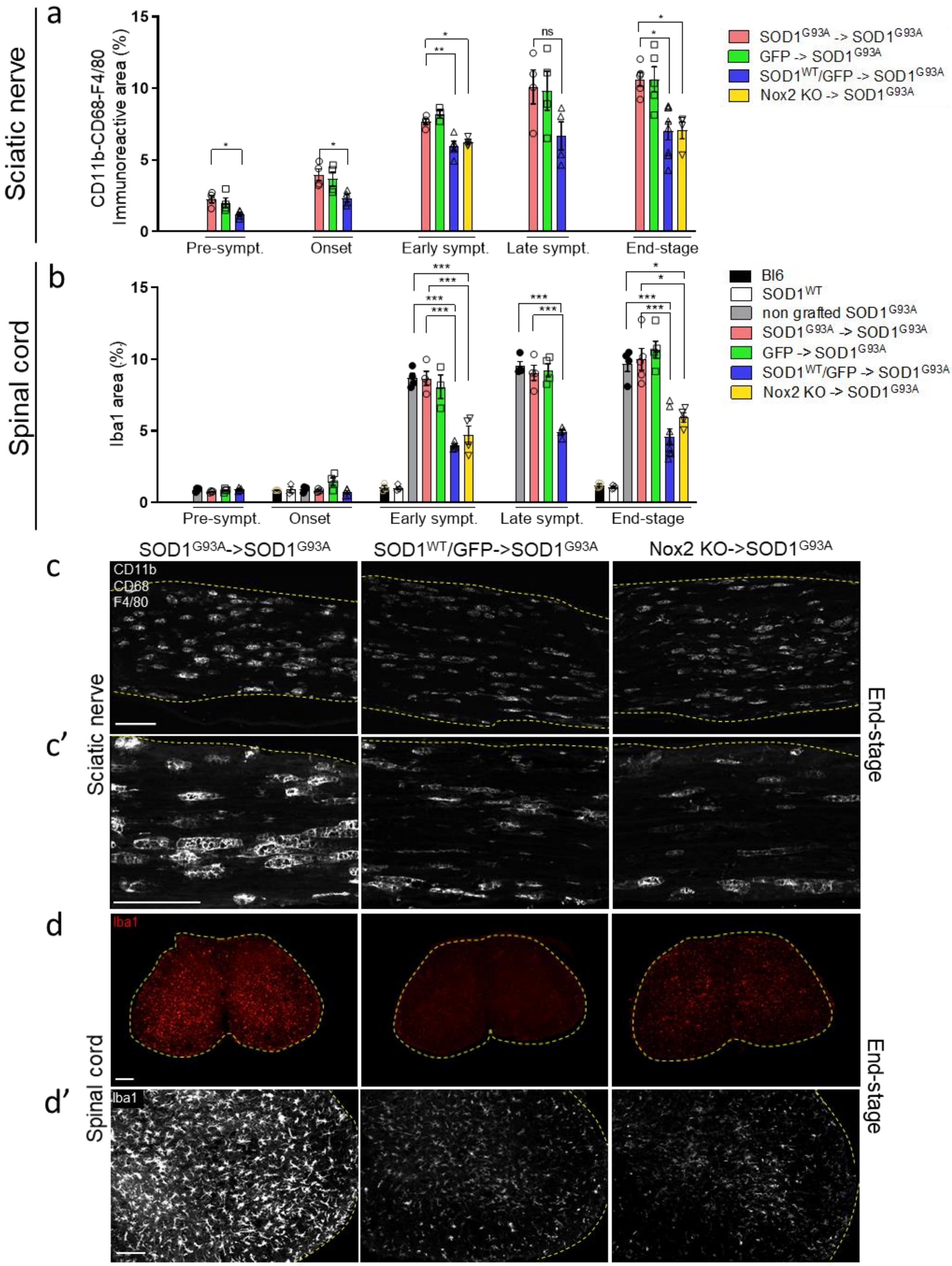

Chiot et al. Figure 3

Fig. 3 | Replacement of peripheral macrophages with SOD1^{WT}/GFP or Nox2 KO BM transplantation decreases peripheral nerve macrophage and CNS microglial activation in ALS mice. **a**, Macrophage activation measured by the CD11b-CD68-F4/80-immunoreactive area in the sciatic nerves of different grafted mice at different disease stages. For control and non-grafted ALS mice, see Fig. 1g and Extended Data Fig. 6g. **b**, Microglial activation measured by the Iba1-immunoreactive area in the lumbar spinal cords of C57Bl6 (Bl6), SOD1^{WT}, non-grafted SOD1^{G93A} and the different groups of SOD1^{G93A}-grafted mice. For **a** and **b**, Nox2 KO→SOD1^{G93A} sciatic nerves and spinal cords were only collected and analyzed at the early-symptomatic and end-stage time points. Data are shown as the mean ± s.e.m.; $*P < 0.05$, $**P < 0.01$, $***P < 0.001$, one-way ANOVA followed by Tukey's post hoc analysis of mean differences; $n = 3$–8 mice per genotype and time point. **c**,**d**, Sciatic nerve (**c**) and spinal cord (**d**) sections of busulfan-treated SOD1^{G93A} mice grafted at a presymptomatic stage (at mean age of 52 days) with BM from SOD1^{G93A} mice (SOD1^{G93A}→SOD1^{G93A}, left), SOD1^{WT}/actin–GFP mice (SOD1^{WT}/GFP→SOD1^{G93A}, middle) and Nox2 KO mice (Nox2 KO→SOD1^{G93A}, right), and stained for the macrophage markers CD11b, CD68 and F4/80 (**c**) or the microglial marker Iba1 (**d**) at disease end-stage. Yellow dashed lines outline the section boundaries. Scale bars, 100 μm.

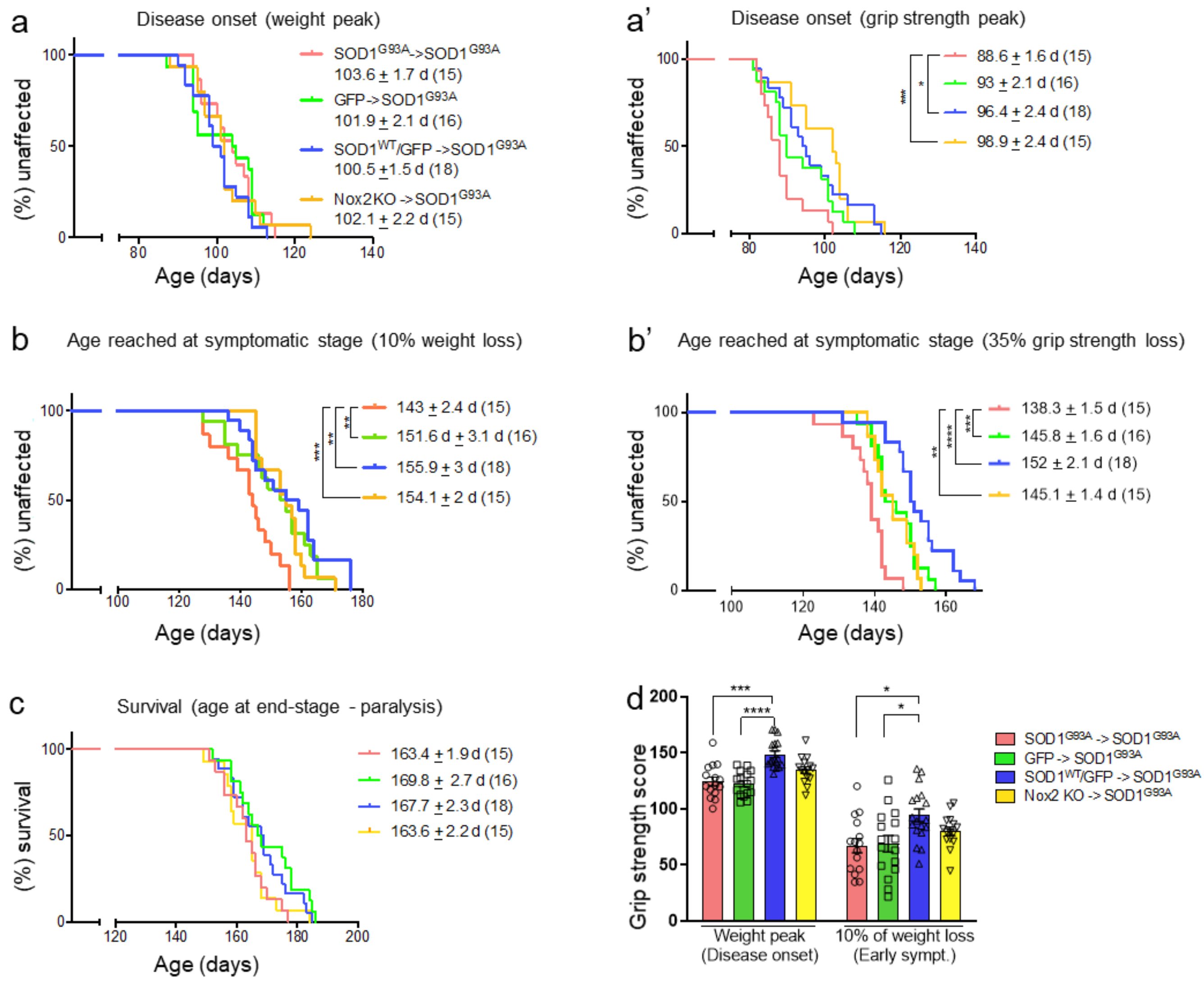

Chiot et al. Figure 4

Fig. 4 | BM transplantation with $SOD1^{WT}$/GFP cells to replace peripheral nerve macrophages at a presymptomatic stage delays the symptomatic disease phase of mutant SOD1-expressing ALS mice. a–**c**, Kaplan–Meier plots of ages reached at onset (at peak weight (**a**, left) or at peak grip strength (**a**, right)), early disease (at 10% of weight loss (**b**, left) or at 35% of grip strength loss (**b**, right)) and end-stage (paralysis (**c**)) in $SOD1^{G93A}$ mice grafted at a presymptomatic stage (at a mean age of 52 days) with $SOD1^{G93A}$ ($SOD1^{G93A}$→$SOD1^{G93A}$), actin–GFP (GFP→$SOD1^{G93A}$), $SOD1^{WT}$/actin–GFP ($SOD1^{WT}$/ GFP→$SOD1^{G93A}$) or Nox2 KO (Nox2 KO→$SOD1^{G93A}$) BM. Mean ages ± s.e.m. are indicated, with the number of animals analyzed in parentheses. The disease course of non-grafted mice is depicted in Extended Data Fig. 8 and was not different from $SOD1^{G93A}$→$SOD1^{G93A}$ mice. **d**, Mean grip strength scores determined at the peak weight (disease onset) and 10% of weight loss (early-symptomatic stage) for different $SOD1^{G93A}$ mouse groups grafted at the presymptomatic stage (n = 15–18 mice). *$P < 0.05$, **$P < 0.01$, ***$P < 0.001$, ****$P < 0.0001$, determined by log-rank test (**a**–**c**) or one-way ANOVA followed by Tukey's post hoc analysis of mean differences (**d**).

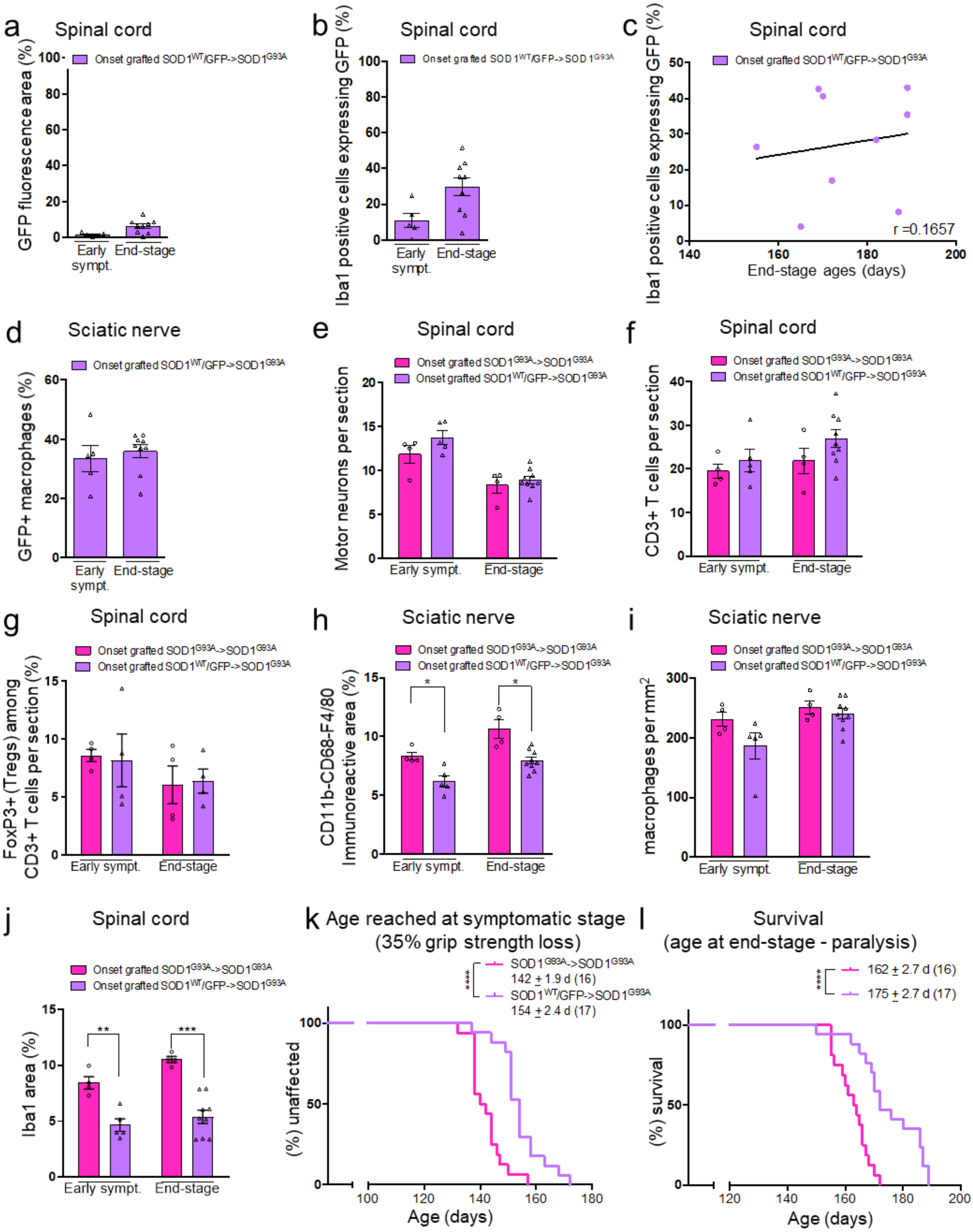

Chiot et al. Figure 5

Fig. 5 | SOD1^{WT}/GFP BM transplantation at disease onset to replace peripheral nerve macrophages increases survival of mutant SOD1-expressing ALS mice. a,**b**, GFP$^+$ cells originating from the periphery in the spinal cord of SOD1^{WT}/GFP→SOD1^{G93A} mice grafted at onset (defined as the mean age of peak weight; 102 days). Data show the area occupied by GFP fluorescence (**a**) and the proportion of Iba1$^+$ microglia expressing GFP (**b**). **c**, Correlation analysis of Iba1$^+$ cells expressing GFP in the spinal cord, with the survival of onset-grafted SOD1^{WT}/GFP→SOD1^{G93A} mice showing no correlation; Spearman coefficient of correlation $r = 0.1657$. **d**, The proportion of GFP$^+$ macrophages among all macrophages (CD11b$^+$CD68$^+$F4/80$^+$) in sciatic nerves of onset-grafted SOD1^{WT}/GFP→SOD1^{G93A} mice. **e**, MN numbers per lumbar spinal cord section. **f**,**g**, The number of T lymphocytes (CD3$^+$, **f**) and the proportion of T_{reg} lymphocytes (Foxp3$^+$, **g**) per spinal cord section. **h**,**i**, The level of macrophage activation as measured by the CD11b-CD68-F4/80-immunoreactive area (**h**) and the number of CD11b$^+$CD68$^+$F4/80$^+$ macrophages (**i**) in sciatic nerves. Note that numbers stayed constant, but activation levels decreased. **j**, The level of microglial activation as measured by the Iba1-immunoreactive area in lumbar spinal cords. Data are shown as the mean ±s.e.m., $n = 4$ SOD1^{G93A}→SOD1^{G93A} mice, $n = 5$ early symptomatic, $n = 9$ end-stage SOD1^{WT}/GFP→SOD1^{G93A} mice (**a**–**j**), except for end-stage SOD1^{WT}/GFP→SOD1^{G93A} mice, $n = 4$ (**g**). $^*P < 0.05$, $^{**}P < 0.01$ $^{***}P < 0.001$, as determined by two-tailed Student's *t*-test (**h** and **j**). **k**,**l**, Kaplan–Meier plots of ages reached at early disease (35% of grip strength loss (**k**), (due to weight loss induced by busulfan/BM treatment at onset; early disease was only defined by grip strength)) and end-stage (paralysis (**l**)). The mean ages ± s.e.m. are indicated, with the number of animals analyzed in parentheses. $^{****}P < 0.0001$, as determined by log-rank test (**k** and **l**).

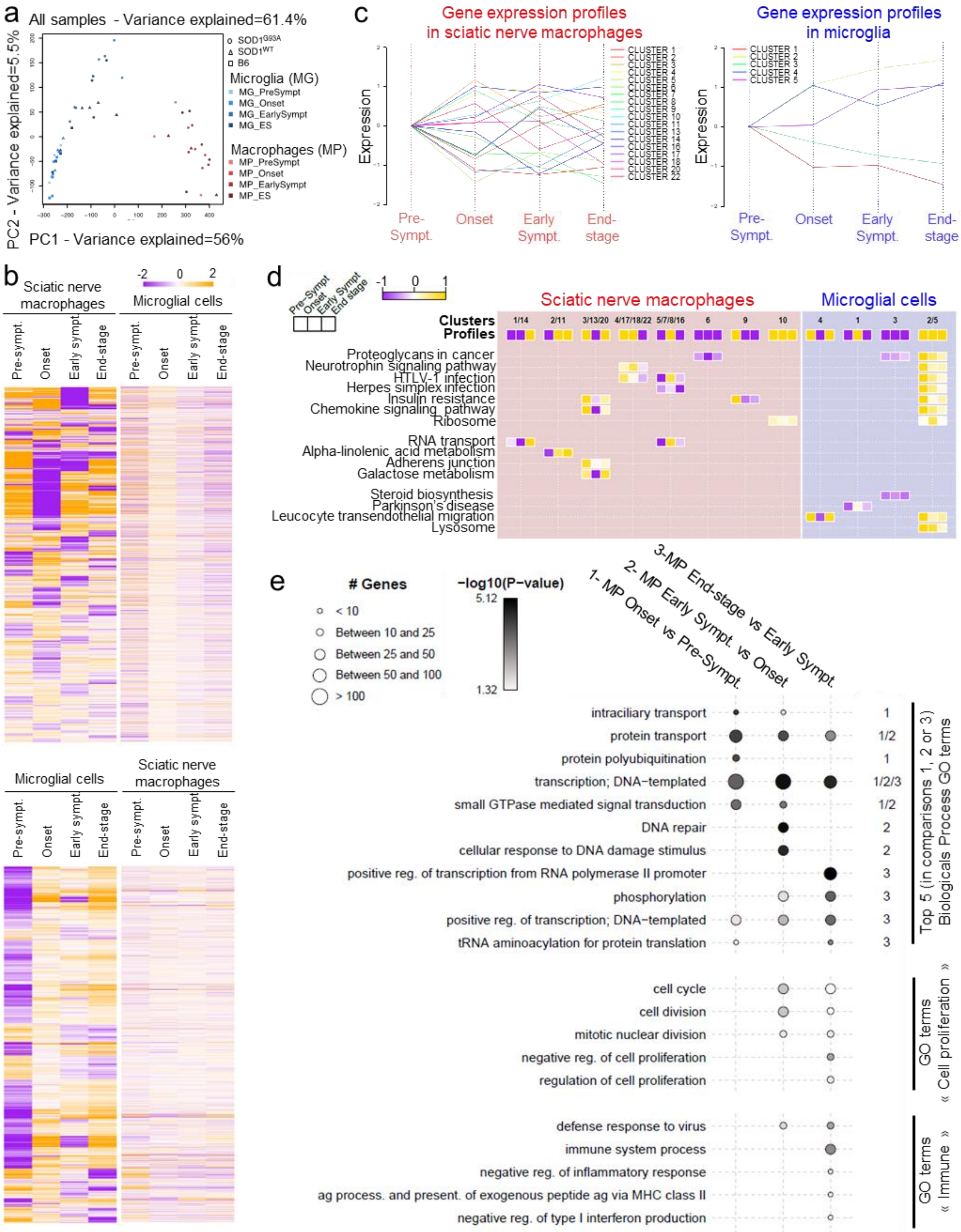

Chiot et al. Figure 6

Fig. 6 | RNA-seq analysis reveals profound differences between reaction profiles of sciatic nerve peripheral macrophages and spinal cord microglia during disease in SOD1^{G93A} ALS mice. a, PCA of all analyzed RNA-seq samples for microglia (blue) and macrophages (red). ES, end-stage. **b**, Top: heatmap of macrophage-regulated genes (regulated between at least two time points) over the disease course (left) and regulation of these macrophage-regulated genes in microglia (right) at the same disease stages. Bottom: heatmap of microglial-regulated genes (between at least two time points) during the disease course (left) and regulation of these microglial-regulated genes in macrophages (right) at the same disease stages. The color scale indicates differences ($\log_2$) in the average expression level among all time points. **c**, Gene expression profiles of sciatic nerve macrophages (left) and microglia (right) depicting the same evolution pattern throughout the disease course, with correlation coefficients of at least $r = 0.6$ (each trace represents a cluster with similar expression profiles). Only clusters with ≥100 genes were selected. **d**, KEGG pathway analyses showing the top pathway for every profile of regulation (upregulated or downregulated along the four time points) as defined by the clustering of expression profiles in **c**. **e**, Detailed GO analyses of nerve-macrophage-regulated genes during disease. Comparisons are between (1) presymptomatic to onset, (2) onset to early symptomatic and (3) early symptomatic to end-stage. EASE score, one-sided modified Fisher exact test for gene enrichment (DAVID v.6.8); exact *P* values are provided in Supplementary Table 7. Ag, antigen; Reg., regulation; Process., processing; Present., presentation.

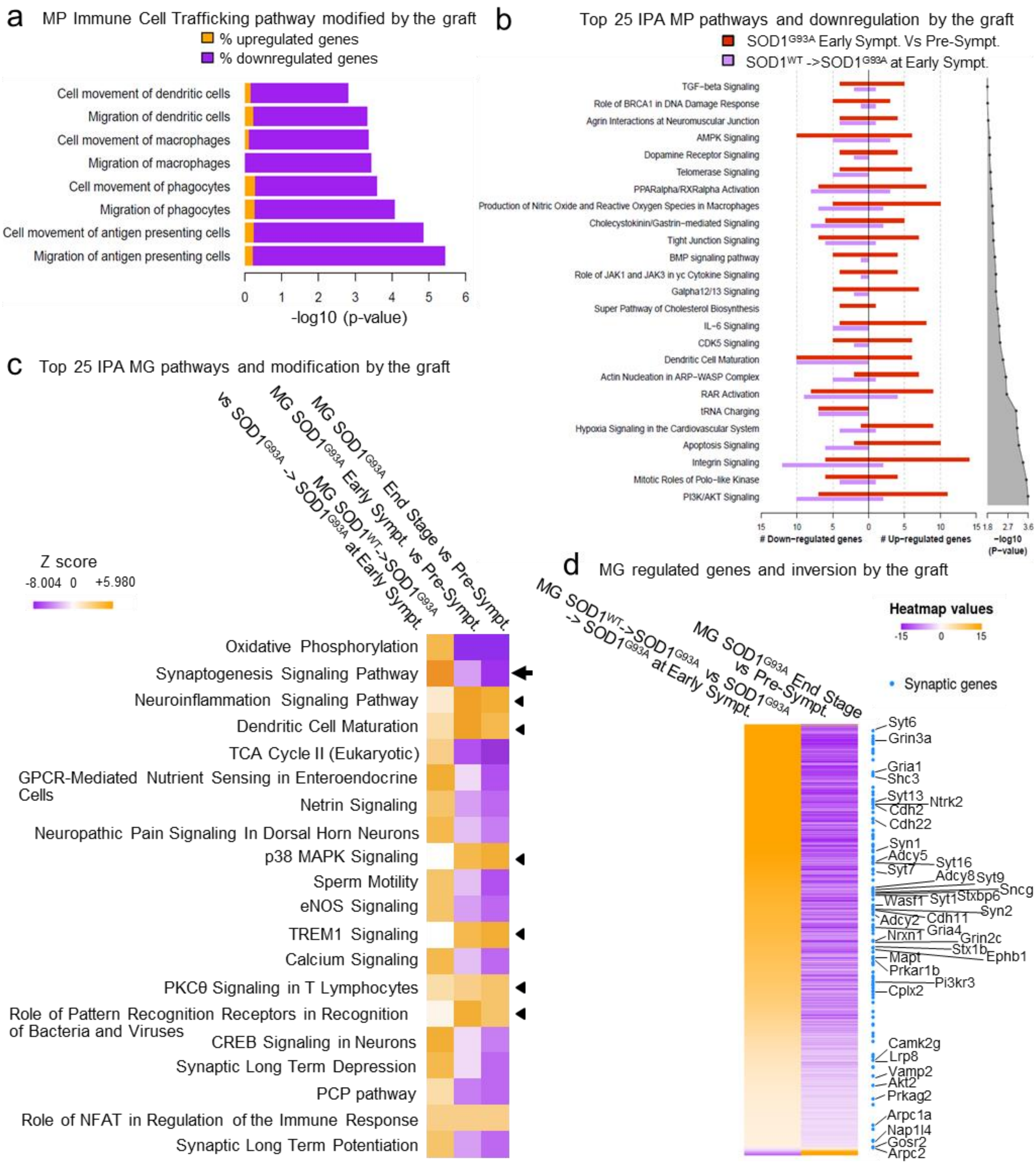

Chiot et al. Figure 7

Fig. 7 | RNA-seq analysis of sciatic nerve peripheral macrophages and microglia isolated from $SOD1^{WT}$/GFP-grafted ALS mice with increased survival reveals a switch in macrophage-activation profiles and modifications of microglial reactivity toward neuronal support. a, The 'immune cell trafficking' pathway (IPA) of sciatic nerve peripheral macrophages from onset-grafted $SOD1^{WT}$→$SOD1^{G93A}$ was compared with $SOD1^{G93A}$→$SOD1^{G93A}$ mice at the early-symptomatic stage. The results showed downregulation of genes by the $SOD1^{WT}$ graft. **b**, The top 25 IPA pathways regulated in macrophages of $SOD1^{G93A}$ mice during the disease course (presymptomatic to early symptomatic) and the effect of the graft in $SOD1^{WT}$→$SOD1^{G93A}$ versus $SOD1^{G93A}$→$SOD1^{G93A}$ macrophages at the early-symptomatic stage. Note that pathways are switched toward downregulation. For **a** and **b**, right-tailed Fisher exact test (IPA software) was performed; exact *P* values are provided in Supplementary Table 7. **c**, The top 25 regulated IPA pathways in $SOD1^{G93A}$ microglia (MG) during disease (presymptomatic to early symptomatic (second lane) or presymptomatic to end-stage (third lane)) and the effect of the graft in $SOD1^{WT}$→$SOD1^{G93A}$ versus $SOD1^{G93A}$→$SOD1^{G93A}$ microglia at the early-symptomatic stage (first lane). Upregulation and downregulation are as defined by the IPA activation *z*-score. Note the downregulation of inflammatory pathways (arrowheads) and the inversion of downregulated pathways toward upregulation, including the 'synaptogenesis signaling pathway' (arrow). **d**, Comparison of all genes regulated in both $SOD1^{G93A}$ microglia during disease (presymptomatic to end-stage) and in $SOD1^{WT}$→$SOD1^{G93A}$ versus $SOD1^{G93A}$→$SOD1^{G93A}$ microglia at the early-symptomatic stage. Note that all 1,049 genes (except one) were inverted, including 120 genes (blue) linked to 'synaptic' GO or IPA terms. Gene symbols are the 39 genes from the IPA 'synaptogenesis signaling pathway'.

EXTENDED FIGURES

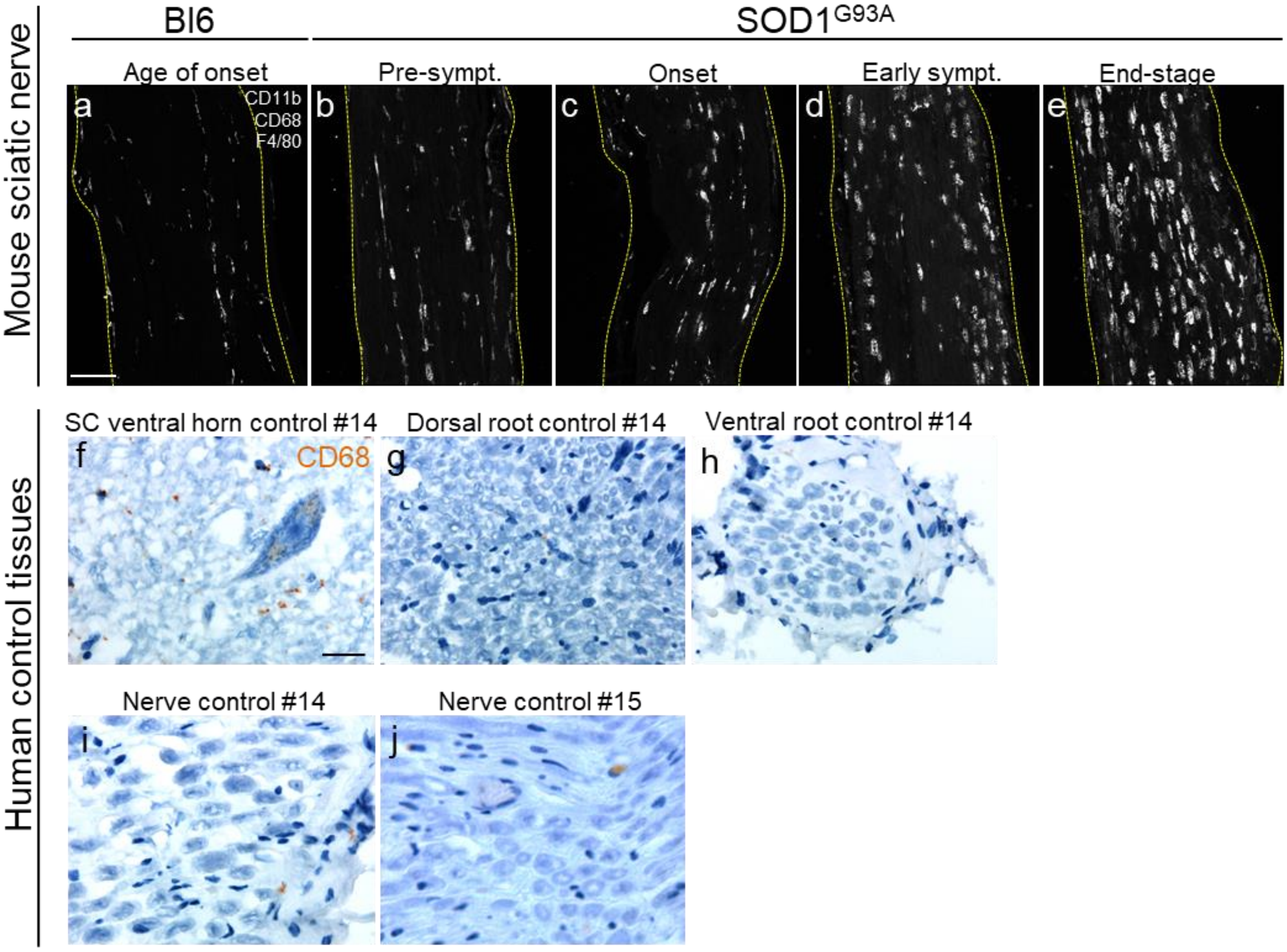

Chiot et al. Extended figure 1

Extended Data Fig. 1 | Staining of macrophages in ALS mouse sciatic nerve and human control spinal cord, root and peripheral nerve tissues. (Additional data to Fig. 1). **a-e**, Immunostaining of sciatic nerves for the macrophage markers CD11b, CD68, F4/80 in 100 day-old control C57Bl6 (Bl6, n = 3 mice) **(a)** and $SOD1^{G93A}$ **(b-e)** mice at different disease stages (n = 4 mice at each stage). Scale bar: 100µm (**a**-**e**). **f-j**, Immunostaining against the microglia/macrophage marker CD68 (in brown) of human control spinal cord ventral horn (**f**), dorsal root (containing sensory neuron axons) (**g**), ventral root (containing motor neuron axons) (**h**) and control peripheral nerves (**i,j**) Scale bars: 40µm (**f**-**j**). Data associated to the n = 11 ALS patients and n = 4 controls in Supplementary Table 1.

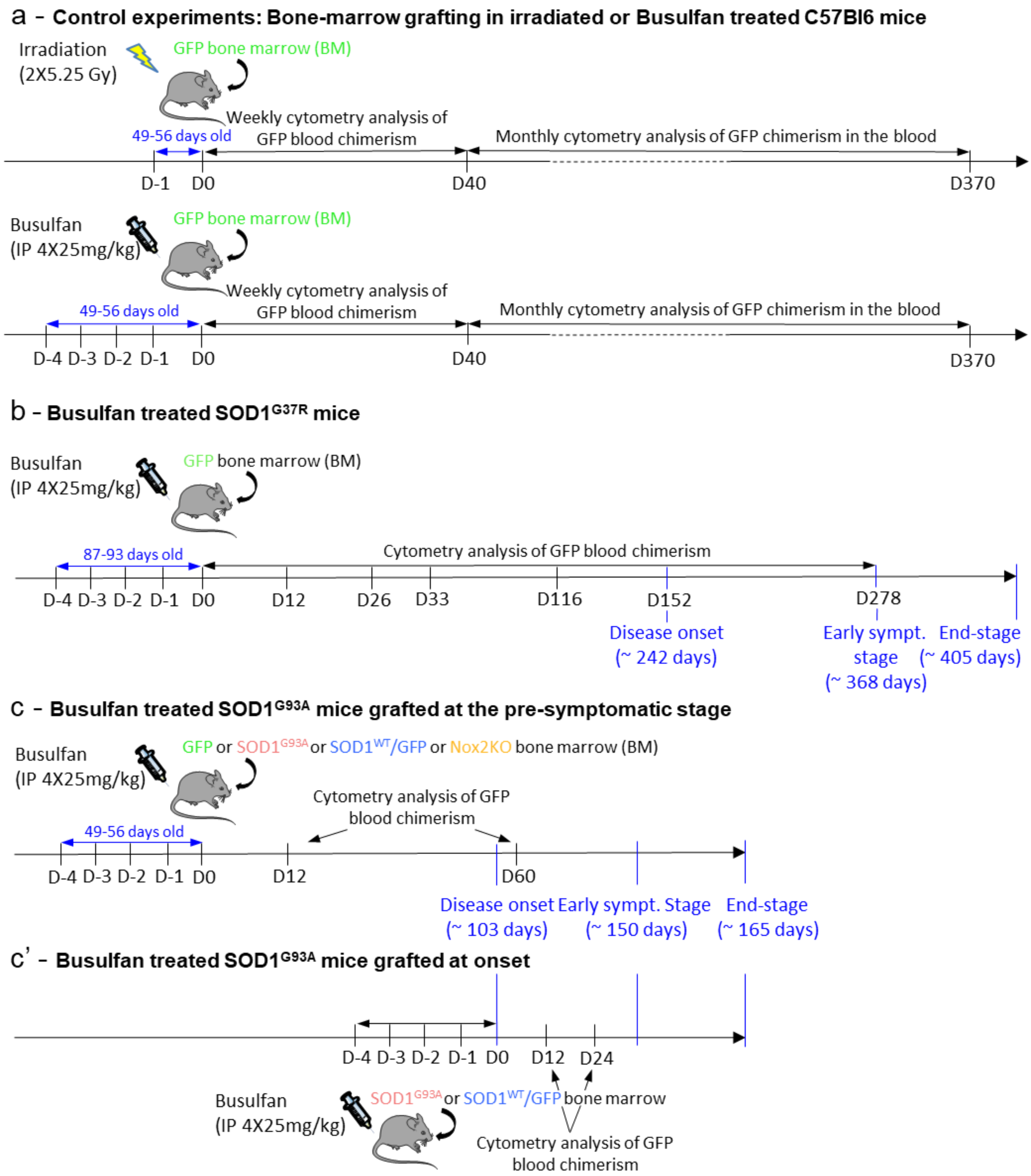

Chiot et al. Extended figure 2

Extended Data Fig. 2 | Scheme of the different bone-marrow (BM) transplantation protocols in control and mutant SOD1 ALS mice. a, Protocols used in control C57Bl6 mice showing the ages at treatments and follow-ups. **b**, Protocol used for busulfan myeloablation and BM transplantation in the slow progressing SOD1^{G37R} mice, indicating the time points when blood GFP+ cells were monitored, and the disease stages. **c-c'**, Protocols used for busulfan myeloablation and BM transplantation in the fast progressing SOD1^{G93A} mice, executed at two different stages, pre-symptomatic (**c**), or at disease onset (**c'**), displaying the time points when blood GFP+ cells were monitored, and the disease stages.

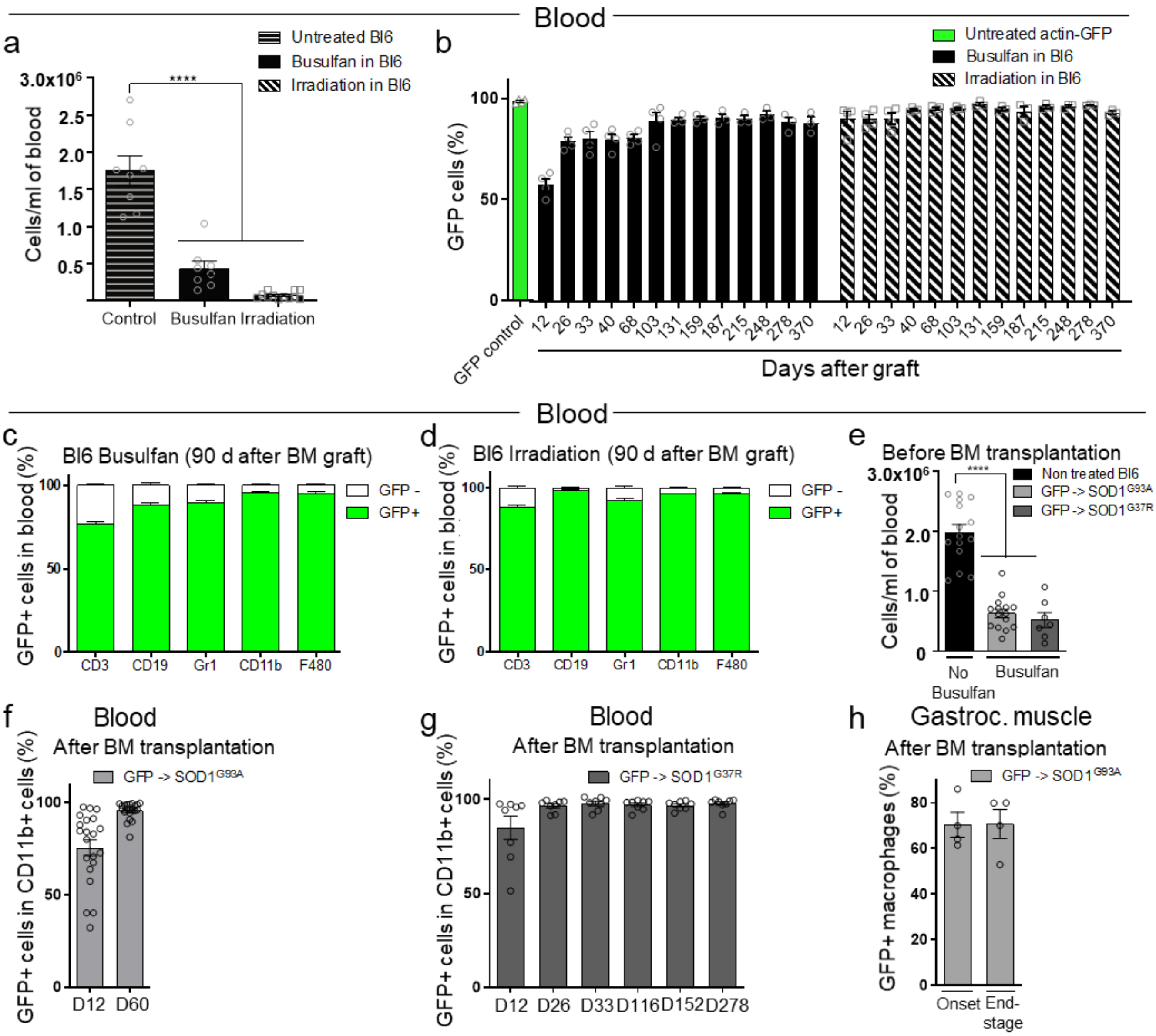

Chiot et al. Extended figure 3

Extended Data Fig. 3 | Analysis of cell replacement in myeloablated and bone-marrow (BM) grafted mice. (Additional data to Fig. 2). **a**, Number of white blood cells /ml of blood in non-treated, busulfan-treated or irradiated C57Bl6 (Bl6) mice; Bars: means±SEM for n = 8–12 mice. ****: $p < 0.0001$, one-way ANOVA followed by a Dunnett's post-hoc analysis. **b**, Proportion of GFP+ cells in the blood of actin-GFP or Bl6 treated mice from D12 to D370 after BM graft. Bars: means±SEM for n = 3-4 mice. **c-d**, Proportion of GFP+ cells in the different blood cell types (CD3+, CD19+,GR1+, CD11b+ and F4/80+ cells) in actin-GFP BM grafted busulfan-treated (n = 4) (**c**) or irradiated (n = 7) (**d**) Bl6 mice. Bars: means±SEM. **e**, Number of white blood cells/ ml of blood after busulfan treatment and before BM graft; bars: means±SEM for n = 7 SOD1^{G37R} mice and n = 15 Bl6 or SOD1^{G93A} mice. ****: $p < 0.0001$, one-way ANOVA followed by a Dunnett's post-hoc analysis. **f-g**, Proportion of GFP+ cells in blood CD11b+ cells of GFP->SOD1^{G93A} mice, 12 and 60 days (corresponding to disease onset) after BM graft (**f**) and of GFP->SOD1^{G37R} mice at several time points after BM graft (**g**); bars: means±SEM for n = 21 **(f)** and n = 8 **(g)** mice. **h**, Proportion of GFP+ macrophages in GFP->SOD1^{G93A} gastrocnemius (Gastroc.) muscles. Bars: means±SEM for n = 4 (onset) or n = 4 (end-stage) mice. Detailed n and statistics in Supplementary Table 7.

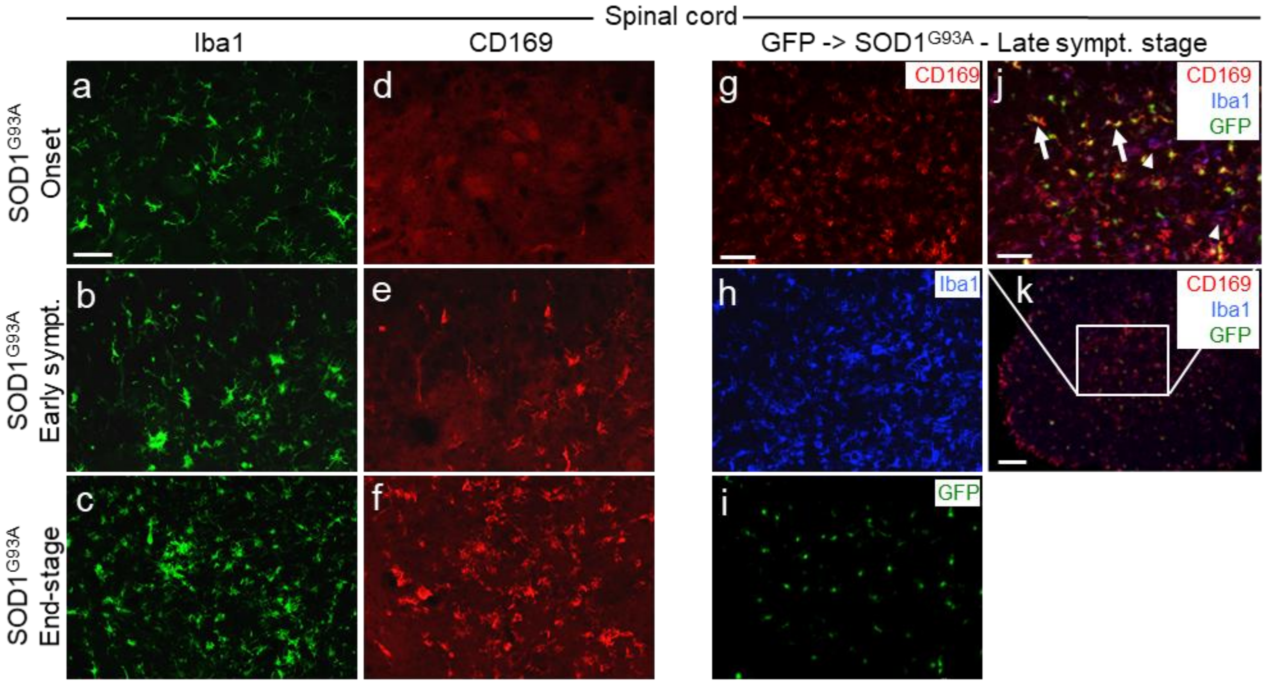

Chiot et al. Extended Figure 4

Extended Data Fig. 4 | Additional analysis for peripheral cell infiltration in the spinal cord of SOD1^{G93A} mice using the Siglec1/CD169 marker previously proposed as peripheral monocyte/macrophage specific. a-f SOD1^{G93A} mouse spinal cord sections immunostained against Iba1 (green; **a-c**) and CD169 (red; **d-f**) at disease onset (n = 4 mice) (**a,d**), early symptomatic stage (n = 4 mice) (**b,e**) and end-stage (n = 4 mice) (**c,f**). Note that CD169 immunostaining was absent at disease onset, as expected, but that CD169 staining increased in Iba1+ cells over the disease course. Scale bar: 50µm (**a-f**). **g-k**, GFP->SOD1^{G93A} mouse spinal cord section at the late symptomatic stage (displaying a higher rate of infiltrated GFP+ cells, n = 3 mice) stained against CD169 (red, **g**) and Iba1 (blue, **h**) and showing GFP+ cells originating from the periphery (green, **i**). **j**, overlay of **(g-i)**, white arrows show GFP+/CD169+/ Iba1+ cells (originating from the periphery), and white arrowheads show non-GFP endogenous microglial cells positive for Iba1 and CD169. **k**, lower magnification of (**j**), white rectangle shows (**j**). Note that CD169 was also expressed by activated microglial cells and that it could therefore not be used to differentiate endogenous microglia from infiltrated peripheral cells. Scale bar: 50µm (for **g-j**), and 100µm (**k**).

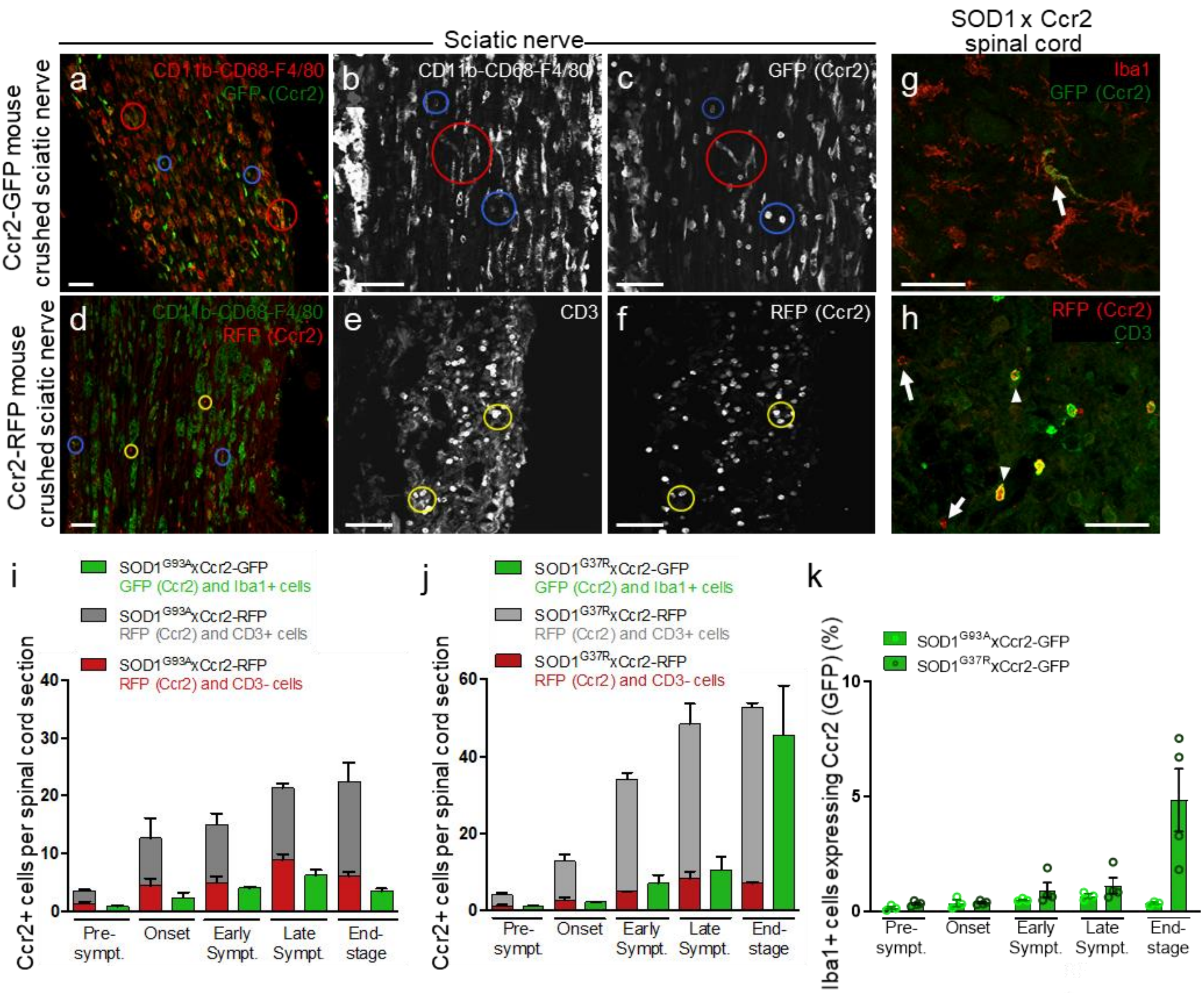

Chiot et al. Extended Figure 5

Extended Data Fig. 5 | Additional analysis for peripheral cell infiltration in the spinal cord of ALS mice using Ccr2-GFP and Ccr2-RFP reporter mice. a–f, Characterization of Ccr2+ cells after sciatic nerve crush-induced inflammation. (**a-c**) Ccr2-GFP mouse sciatic nerves (n = 3 mice). Blue circles show GFP+ (Ccr2+, green) and (CD11b-CD68-F4/80)+ (red) monocytes and red circles show GFP+/(CD11b, CD68, F4/80)+ differentiated macrophages (identified by their morphology). (**d-f**) Ccr2-RFP mouse sciatic nerves (n = 4 mice). (**d**) Blue circles show (CD11b-CD68-F4/80)+ (green)/RFP (Ccr2)+ (red) monocytes, yellow circles show RFP (Ccr2)+ cells but not expressing the macrophage markers. **(e-f)** To identify these cells, Ccr2-RFP sciatic nerves were stained against the pan T cell marker CD3 (**e**) and against RFP (**f**) showing that most of the RFP+ (Ccr2+) cells in Ccr2-RFP mouse sciatic nerves, after a lesion, are T lymphocytes (yellow circle). Scale bars: 100 μm (**a**,**d**) and (**b**-**c**, **e**-**f**). **g-h**, Characterization of Ccr2+ cells in spinal cords of SOD1^{G93A} mice crossed with Ccr2-GFP mice (n = 3) (**g**) or Ccr2-RFP mice (n = 4) (**h**) at disease end-stage. **g**, white arrow points to an Iba1+ (red) Ccr2+ (anti-GFP- green) cell. **h**, White arrowheads: CD3+/RFP+ cells (lymphocytes expressing Ccr2), white arrows: CD3-/ RFP+ monocytes showing that most of the RFP+ (Ccr2 positive) cells in Ccr2-RFPxSOD1 mice were T lymphocytes. Scale bar: 50μm (**g**,**h**). **i-j**, Quantifications of CCR2+Iba+ and CD3- monocytes/ macrophages or CD3+ lymphocytes originating from the periphery in Ccr2-GFPxSOD1^{G93A} (**i**, n = 3-4 mice/time point) and Ccr2-GFPxSOD1^{G37R} (**j**, n = 4 mice/ time point) mice. **k**, Proportion of Iba1+ myeloid cells expressing Ccr2 (GFP+) in Ccr2-GFPxSOD1^{G93A} (n = 3 mice/time point) and Ccr2-GFPxSOD1^{G37R} (n = 4 mice/time point) mice. Bars: means± SEM. Detailed n and statistics in Supplementary Table 7.

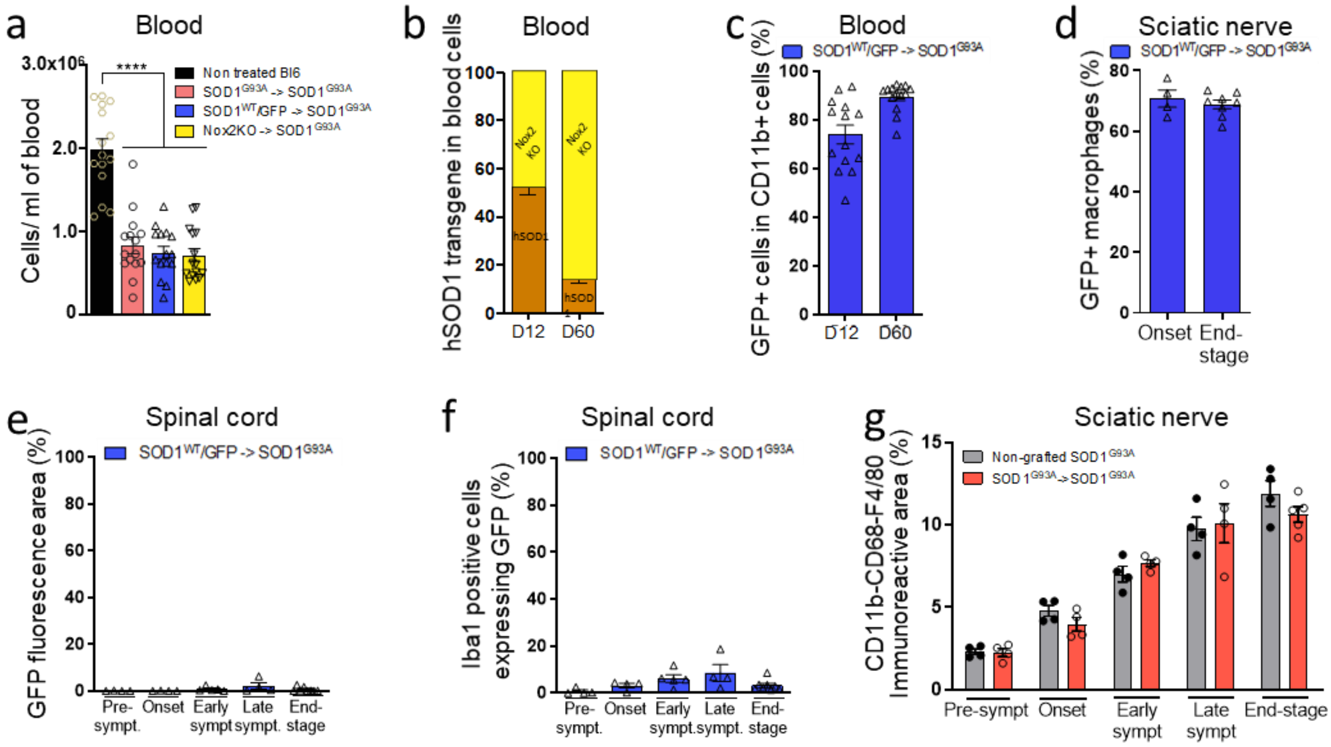

Chiot et al. Extended figure 6

Extended Data Fig. 6 | Further characterization of the bone-marrow (BM) transplanted ALS mice and the pathology in their tissues. (Additional data to Figs. 3 and 4). **a**, Number of white blood cells per ml of blood in non-treated C57Bl6 (Bl6) mice and busulfan-treated mice before BM transplantation. Bars represent means±SEM for n = 15 mice per group. ****: $p < 0.0001$, one-way ANOVA followed by a Dunnett's post-hoc analysis. **b**, As Nox2 KO cells do not express human SOD1, cells originating from the Nox2 KO BM were indirectly identified by measuring, in the blood cells of Nox2 KO->SOD1^{G93A} mice, the levels of human SOD1 transgenes by a quantitative PCR, 12 days and 60 days after BM transplantation. Bars: means±SEM for n = 12 mice/time point. Lower levels of human SOD1 in the blood revealed higher levels of Nox2 KO cells. **c**, Proportion of GFP+ cells in CD11b+ myeloid cells in the blood of SOD1^{WT}/GFP->SOD1^{G93A} mice 12 days and 60 days after BM transplantation. Bars: means±SEM for n = 14 mice at each time point. **d**, Proportion of GFP+ macrophages among all (CD11b-CD68-F4/80) + macrophages in the sciatic nerves of SOD1^{WT}/GFP->SOD1^{G93A} mice. Means±SEM for n = 4 (onset) and n = 8 (end-stage) mice. **e**, **f**, Quantification of GFP+cells originating from the periphery in the spinal cord of SOD1^{WT}/GFP->SOD1^{G93A} mice at the different disease stages. **e**, Area occupied by GFP fluorescence and **f**, proportion of Iba+ microglial cells expressing GFP. Bars represent means±SEM for n = 3–8 mice per time point and genotype. **g**, Macrophage activation measured by CD11b-CD68-F4/80 immunoreactive area in sciatic nerves of non-grafted SOD1^{G93A} (grey, same data as Fig. 1g) and SOD1^{G93A}->SOD1^{G93A} (red, same data as Fig. 3a) mice. Bars represent means±SEM for n = 4-5 mice per genotype and time point. Detailed n and statistics in Supplementary Table 7.

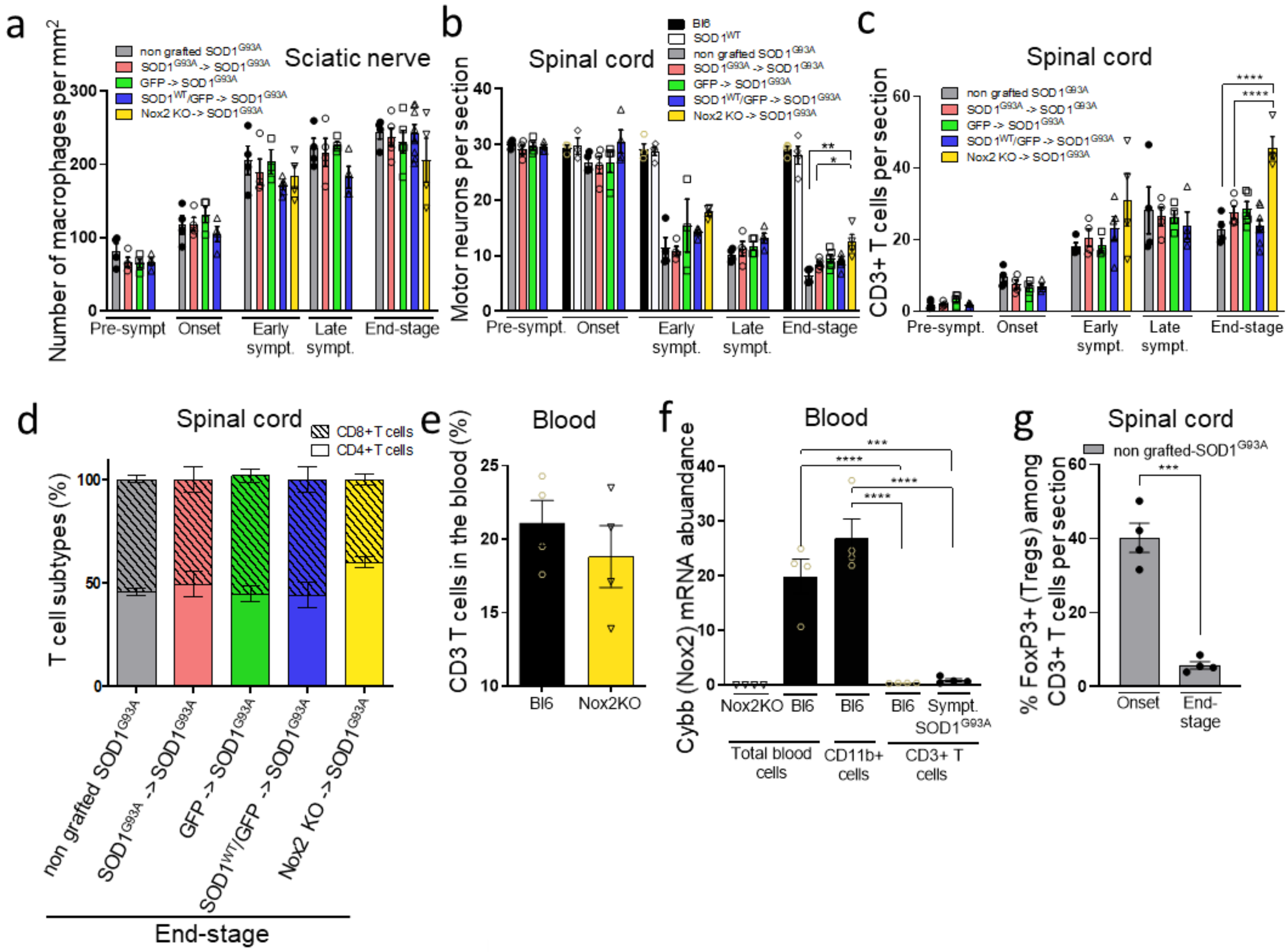

Chiot et al. Extended figure 7

Extended Data Fig. 7 | Additional analysis of pre-symptomatic grafted SOD1^{G93A} mice. (Additional data to Figs. 3 and 4). **a**, Density of macrophages (in cells/mm^2) in sciatic nerves of non-grafted SOD1^{G93A} and pre-symptomatic grafted SOD1^{G93A} mice, at the different disease stages. **b**, motor neuronnumbers per spinal cord section in C57Bl6 (Bl6), SOD1^{WT}, non-grafted SOD1^{G93A} and pre-symptomatic grafted SOD1^{G93A} mice. **c**, Number of T lymphocytes (CD3+) per lumbar spinal cord section of non-grafted and pre-symptomatic grafted SOD1^{G93A} mice. Bars: means±SEM; n = 3–8 mice per genotype and time-point (**a-c**). **d**, Ratio of CD4+ and CD8+T cells in the spinal cord of non-grafted and pre-symptomatic grafted SOD1^{G93A} mice at end-stage. Note that Nox2 KO->SOD1^{G93A} mice were the only ones showing increased number of lymphocytes and that CD4+ cells were predominant. Bars: means±SEM for n = 4–8 mice/group. **e**, Proportion of T lymphocytes (CD3+) in the blood of control Bl6 and Nox2 KO mice. Bars: means±SEM for n = 4 mice/ group. **f**, *Cybb* (encoding for Nox2) mRNA levels in blood cells of Nox2 KO, Bl6 and symptomatic SOD1^{G93A} mice. Bars: means±SEM for n = 4 mice/group. Note that T lymphocytes barely expressed Nox2 in control and symptomatic SOD1^{G93A} mice - deletion of Nox2 in T lymphocytes was unlikely to influence their infiltration, which was rather linked to a non-cell autonomous effect. **g**, Proportion of regulatory T lymphocytes (FoxP3+ and CD3+) among T lymphocytes (CD3+) in the spinal cord of non-grafted SOD1^{G93A} mice at onset and end-stage. Bars: means±SEM for n = 4 mice/group. *: $p < 0.05$; **: $p < 0.01$; ***: $p < 0.001$; ****: $p < 0.0001$, one-way ANOVA followed by a Tukey's post-hoc analysis (**b, c, f**), and two tailed student t-test (**g**). Detailed n and statistics in Supplementary Table 7.

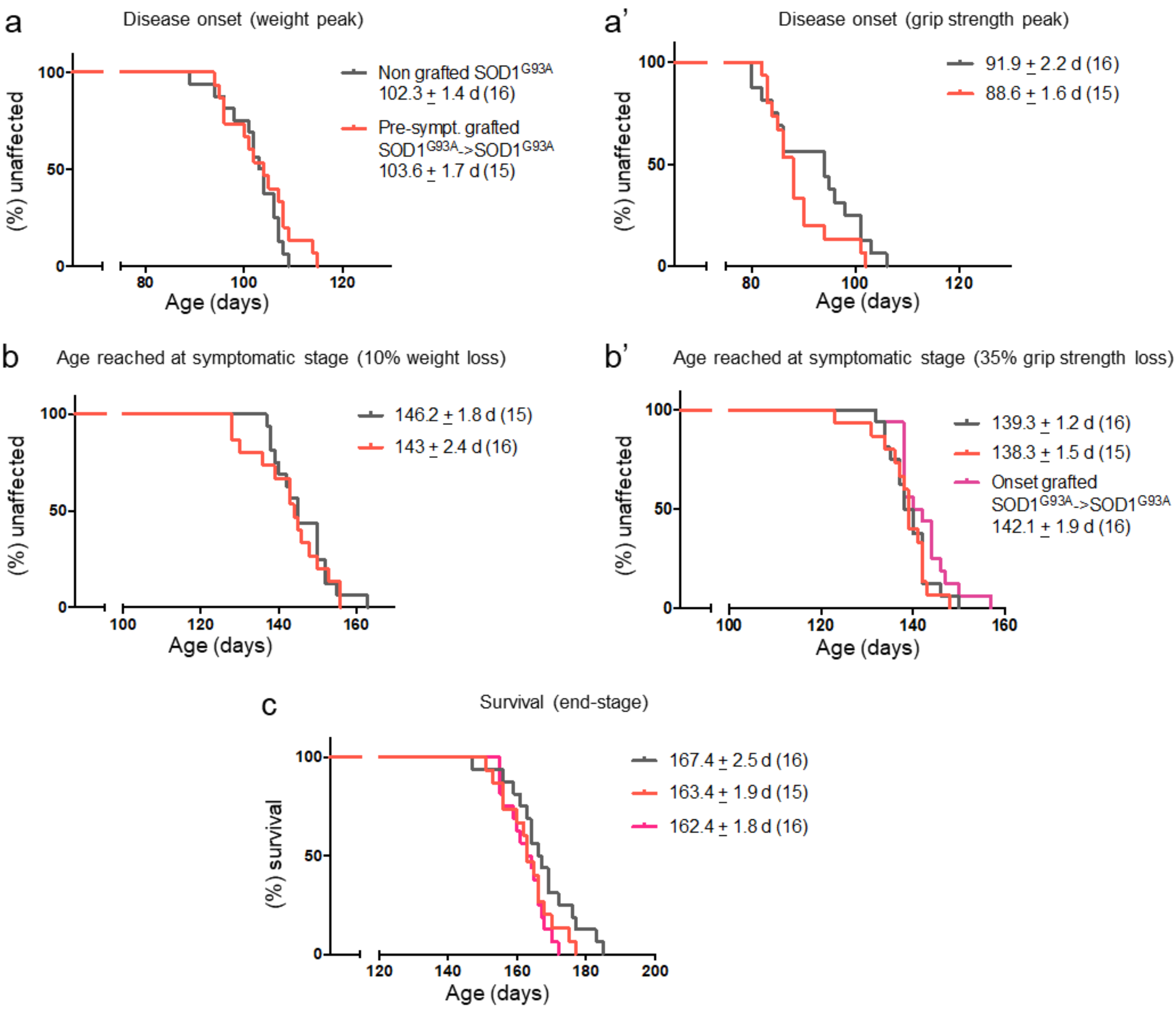

Chiot et al. Extended figure 8

Extended Data Fig. 8 | SOD1^{G93A} bone-marrow transplantation at the pre-symptomatic stage or at onset does not influence disease progression of SOD1^{G93A} ALS mice, showing no influence of the transplantation protocol, per se. (Additional data to Figs. 3, 4 and 5). **a-c**, Kaplan-Meier plots of ages reached at onset [at weight peak (**a**) or at grip strength peak (**a'**)], early disease [at 10% of weight loss (**b**) or at 35% of grip strength loss (**b'**)] and end-stage [at complete hind limb paralysis (**c**)], in non-grafted SOD1^{G93A} mice (grey), SOD1^{G93A} bone-marrow grafted SOD1^{G93A} (SOD1^{G93A}->SOD1^{G93A}) mice, grafted at the pre-symptomatic stage (red) or at disease onset (pink). Mean ages±SEM are indicated with animal numbers in brackets. No statistical significant differences were found between the groups at any time-point, according to log-rank test.

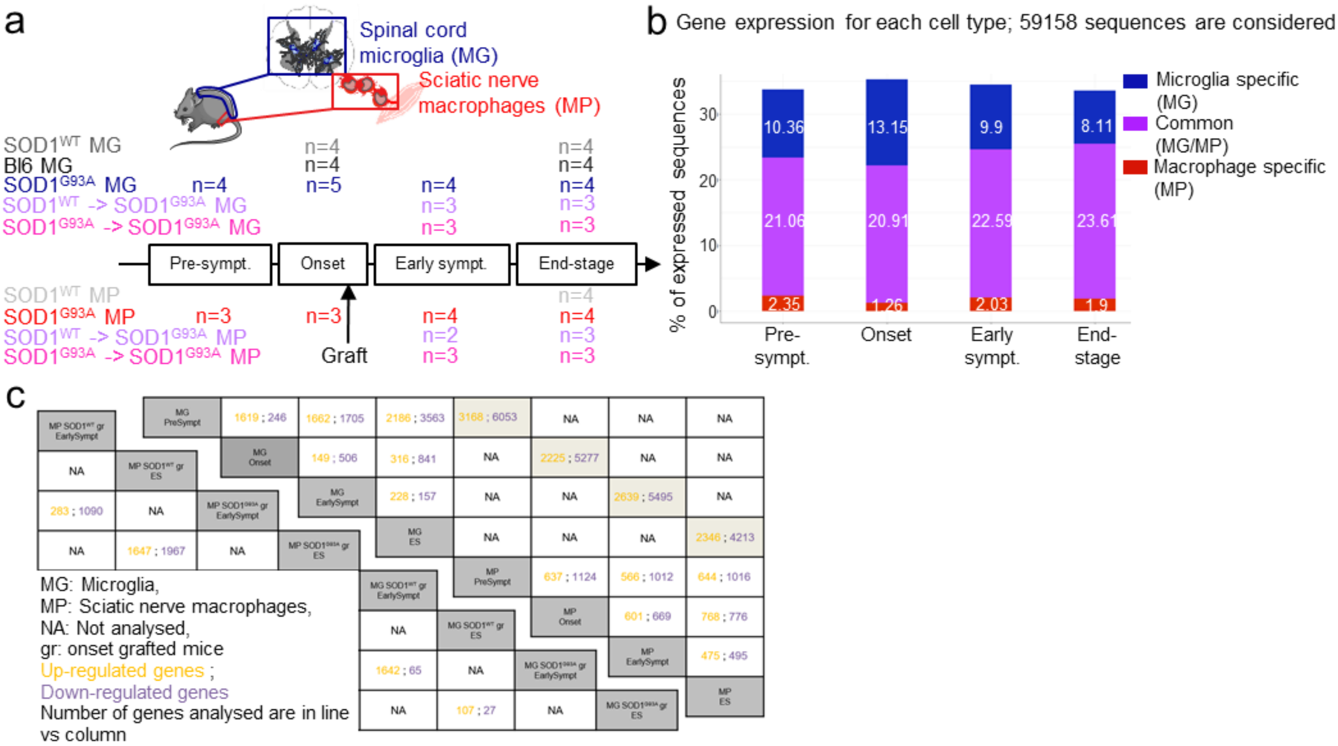

Chiot et al. Extended Figure 9

Extended Data Fig. 9 | Additional analysis of RNAseq data obtained from sciatic nerve macrophages and spinal cord microglia. (Additional data to Figs. 6 and 7). **a**, Scheme depicting the different groups and numbers of samples analyzed by RNA sequencing (RNAseq). Microglial cells (MG) were isolated from SOD1^{G93A}, SOD1^{WT}, C57Bl6 (Bl6) and onset grafted SOD1^{WT}->SOD1^{G93A} and SOD1^{G93A}->SOD1^{G93A} mice. Sciatic nerve peripheral macrophages (MP) were isolated from SOD1^{G93A} mice at the 4 stages, onset grafted SOD1^{WT}->SOD1^{G93A} and SOD1^{G93A}->SOD1^{G93A} at 2 stages and from SOD1^{WT} mice at the age corresponding to disease end-stage in SOD1^{G93A} mice, but could not be recovered from Bl6 mice probably due to their limited numbers. **b**, Percentage of sequences specific to microglia (blue) or sciatic nerve peripheral macrophages (red) or common to both (purple), at the different disease stages. Only genes expressed in at least two samples per group were considered. **c (right panel)**, Table summarizing the number of regulated genes (up-regulated, yellow; down-regulated, purple) between the different disease stages in SOD1^{G93A} microglial cells (MG) or sciatic nerve peripheral macrophages (MP), and at equivalent stages between SOD1^{G93A} microglial cells and sciatic nerve peripheral macrophages (grey boxes). **c (left panel)**, Table summarizing the number of regulated genes (up-regulated, yellow; down-regulated, purple) in microglial cells (MG) or sciatic nerve peripheral macrophages (MP), between onset grafted SOD1^{WT}->SOD1^{G93A} and SOD1^{G93A}->SOD1^{G93A} mice at early symptomatic stage or disease end-stage. ES: end-stage.

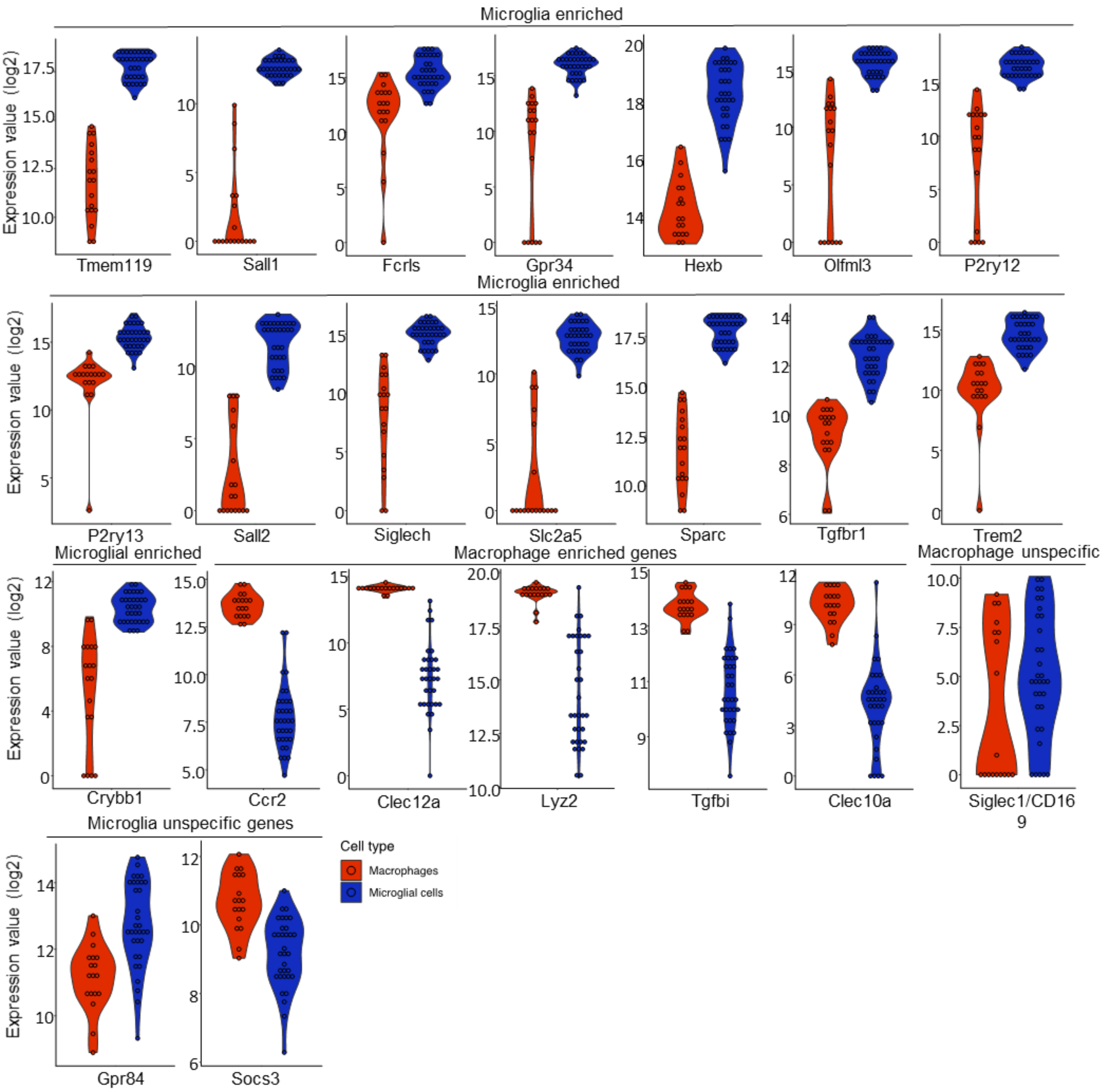

Chiot et al. Extended Figure 10

Extended Data Fig. 10 | Analysis of microglia and macrophage specific genes in RNAseq data obtained from spinal cord microglia and sciatic nerve macrophages. (Additional data to Figs. 6 and 7). Violin plots of all values at all the control/disease stages for nerve macrophages (red) or microglia (blue) of 15 microglia and 5 macrophage signature genes. Signature gene references: Chiu, I. M. *et al*. A neurodegeneration-specific gene-expression signature of acutely isolated microglia from an amyotrophic lateral sclerosis mouse model. *Cell Rep*. 4, 385–401 (2013)[22]; Bennett, F. C. *et al*. A Combination of Ontogeny and CNS Environment Establishes Microglial Identity. *Neuron* 98, 1170–1183 (2018)[23]; Bennett, M. L. *et al*. New tools for studying microglia in the mouse and human CNS. *Proc. Natl. Acad. Sci*. 12, E1738–E1746 (2016)[24]; Zondler, L. *et al*. Peripheral monocytes are functionally altered and invade the CNS in ALS patients. *Acta Neuropathol*. 132, 391–411 (2016)[25]; Van Hove, H. *et al*. A single-cell atlas of mouse brain macrophages reveals unique transcriptional identities shaped by ontogeny and tissue environment. *Nat. Neurosci*. 22, (2019)[62]; Saederup, N. *et al*. Selective chemokine receptor usage by central nervous system myeloid cells in CCR2-red fluorescent protein knock-in mice. *PLoS One* 5, (2010)[54], Lund, H. *et al*. Competitive repopulation of an empty microglial niche yields functionally distinct subsets of microglia-like cells. *Nat. Commun*. 9, 4845 (2018)[63]; Gosselin, D. *et al*. An environment-dependent transcriptional network specifies human microglia identity. *Science*. 3222, 33–35 (2017)[64].

Methods

Animals. All the mice were on a C57Bl6/J genetic background (Bl6; Janvier Labs). The following SOD1 transgenic mouse lines were used: hSOD1^{G93A} mice (B6.Cg-Tg(SOD1*G93A)1Gur/J; 004435, Jackson Laboratory)[2]; hSOD1^{G37R} mice (the previously described hSOD1^{G37R} line in which the h*SOD1* transgene is flanked by *loxP*)[3]; and hSOD1^{WT} mice (B6.Cg-Tg(SOD1)2Gur/J; 002298, Jackson Laboratory)[2]. SOD1^{G37R} mice were provided by D. W. Cleveland (UCSD, USA). SOD1^{WT} mice were used as control mice for the overexpression of the human *SOD1* transgene and, although they have been reported to develop some signs of MN degeneration but only at very advanced ages[51], they do not develop any evident motor phenotype or paralysis. SOD1^{G93A} and SOD1^{G37R} mice develop an ALS-like phenotype, including progressive paralysis. ALS mice were hemizygous for a 12-kb genomic fragment encoding the human wild-type or mutated *SOD1* gene under its endogenous promoter. Mice carrying the human *SOD1* transgene were identified by PCR screening of tail DNA using a mouse *SOD1* forward primer (5′-GTTACATATAGGGGTTTA CTTCATAATCTG-3′), a human *SOD1* forward primer (5′-CCAAGA TGCTTAACTCTTGTAATCAATGGC-3′) and a mouse and human *SOD1* reverse primer (5′-CAGCAGTCACATTGCCCAGGTCTCCAACATG-3′), resulting in a ~800 bp mouse and a ~600 bp human *SOD1* PCR product. The following mouse lines were used as donors for the BM transplantation experiments: actin–GFP transgenic mice (C57Bl/6-Tg(CAG-EGFP)1Osb/J; 003291, Jackson Laboratory) expressing enhanced GFP complementary DNA under the control of the chicken beta actin promoter and therefore ubiquitously expressing GFP; Nox2 KO mice (B6.129S-Cybbtm1Din/J; 002365, Jackson laboratory)[52]; and SOD1^{WT}/ GFP mice, resulting from crossing heterozygous SOD1^{WT} with homozygous actin–GFP mice. The following two mouse lines were used for macrophage tissue infiltration studies expressing either GFP or RFP under the mouse *Ccr2* promoter: BAC transgenic *Ccr2*–GFP mice[53], identified by PCR screening of tail DNA using a *Ccr2*–GFP forward primer (5′-AATGGCGCAAGGCTATTTGG-3′) and a *Ccr2*–GFP reverse primer (5′-CGGCGAGCTGCACGCTGCGTCCTC-3′); and *Ccr2*–RFP knock-in mice (B6.129(Cg)-Ccr2tm2.1Ifc/J; 017586, Jackson Laboratories)[54], identified by PCR screening of tail DNA using a common *Ccr2* forward primer (5′- TAAACCTGGTCACCACATGC-3′), a *Ccr2* reverse primer (5′- GGAGTAGAGTGGAGGCAGGA-3′) and a RFP reverse primer (5′-CTTGATGACGTCCTCGGAG-3′). Housing conditions were as follows: temperature 20 ± 2 °C; humidity: 55 ± 10%; light–dark cycle: 12 h–12 h; ventilation: approximately 12 cycles per hour of filtered, non-recycled air. All animal procedures (including end-stage definition) were performed in accordance with the guidelines for the care and use of experimental animals of the European Union and approved by the ethics committee for animal experimentation number 5 of Ile-de-France.

Disease-stage analysis. Mice were followed weekly from the presymptomatic stage (around 50 days for SOD1^{G93A} mice and 90 days for SOD1^{G37R} mice) until disease end-stage (around 165 days for SOD1^{G93A} mice and 405 days for SOD1^{G37R} mice). Mice were followed for signs of paralysis, and their grip strength was measured (Bioseb, grip test; average of three consecutive weekly measures); mice were also weighed weekly as an objective and unbiased measure of disease course[3,55]. Grip-strength measures were used until the animal was too weak to perform this test and reached a force of around 30–40 *g*, which corresponded to around the late-symptomatic stage. For tissue analyses of grafted GFP→SOD1^{G37R} mice, tissues were all from females except for animals at end-stage, and half of the animals analyzed at the early-symptomatic stage, which were males. Non-grafted SOD1^{G93A}, grafted SOD1^{G93A}→SOD1^{G93A}, GFP→SOD1^{G93A}, SOD1^{WT}/GFP→SOD1^{G93A}, Nox2

KO→SOD1^{G93A} mouse cohorts, C57Bl6, and SOD1^{WT} cohorts were composed of all females only. SOD1^{G37R}×Ccr2–GFP mice were females, except for the early-symptomatic and end-stage groups, which were composed of three females and one male. SOD1^{G37R}×Ccr2–RFP mice were equally gender mixed, except for presymptomatic and end-stage groups, which were composed of three females and one male. SOD1^{G93A}×Ccr2–GFP mice were females, except for the onset and late-symptomatic groups, which were composed of three females and one male. SOD1^{G93A}×Ccr2–RFP mice were equally gender mixed, except for the presymptomatic group, which was composed of females, and the early-symptomatic group, which was composed of three females and one male. We verified that within all the groups, the distribution of the data was not linked to gender. Disease time points were defined as follows. The time of disease onset was retrospectively determined as the time when mice reached either peak body weight or peak grip strength. The time of early disease was defined as the age at which the animals had lost 10% of their maximal weight or 35% of their maximal grip strength, which is accompanied by gait alterations and failure of the hindlimb splaying reflex, but without obvious signs of paralysis. This early disease stage was followed by the appearance of progressive paralysis. The late-symptomatic stage was considered when mice had lost 15% of their maximal weight. This stage was characterized by the beginning of hindlimb paralysis, walking difficulties and inability to perform the grip test. During the symptomatic phase, mice were observed at least twice a week and daily when they approached end-stage, which was defined by paralysis so severe that the animal could not right itself within 20 s when placed on its side, an end point frequently used for mutant SOD1- mice. The mean ages ± s.e.m. of the different disease stages in SOD1^{G93A} mice were as follows: disease onset: 102.3 ± 1.4 days; early-symptomatic stage: 146.2 ± 1.8 days; and disease end-stage: 167.4 ± 2.5 days. Concerning SOD1^{G37R} mice, the mean ages were as follows: disease onset: 247 ± 6.5

days; early-symptomatic stage: 360.5 ± 7.7 days; and disease end-stage 405.7 ± 7.5 days. Kaplan–Meier analysis was used for survival curves. Log-rank tests were used for statistical analysis.

Sciatic nerve crush. Mice were placed under isofluorane anesthesia and the sciatic nerve was exposed via an incision in the flank followed by the separation of underlying muscles. The sciatic nerve was crushed, twice for 5 s, at two apposed locations using fine jewelers' forceps at the level of the obturator tendon. Functional recovery was assessed by daily measurement of the toe spread (the length between the first and the fifth digit) of the operated limb compared with the control limb. Full recovery of the nerve usually takes 2–3 weeks, and tissue analysis was performed 7 days after the crush, when strong inflammation was present.

Cytometry analysis. Blood samples (100 µl) were collected in EDTA-coated tubes from the retro-orbital sinus and mixed with 100 µl (1:1) of 0.1 M HBSS supplemented with 1% FCS (low endotoxins, Life Technologies). Blocking was performed using Fc Block (anti-CD16/CD32, 1:200, BD Biosciences). Leukocytes were labeled using anti-CD11b-PE (1:200, BD Pharmingen), anti F4/80-PE-cyanine 5 (1:200, e-Bioscience), anti-CD3-APC cyanine 7 (1:200, BD Pharmingen), anti-CD19-Alexa Fluor 700 (1:200, BD Pharmingen) and anti-Ly6C/ Ly6G-V450 (1:200 BD Biosciences) antibodies. Red blood cells were lysed in 2 ml of fixative BD FACS lysing solution (1/10 in water, BD Biosciences). Cytometry was performed on a FACSVerse cytometer (BD Biosciences) and data were analyzed using FlowJo software.

BM transplantation. *Myeloablative conditioning.* Mouse recipients received an intraperitoneal injection of the alkylating agent busulfan (Busilvex, stock concentration of 6 mg ml^{-1}), which targets cycling cells (and is expected to target macrophages responding to neurodegeneration in the affected tissues of ALS mice), at the age of 49–56 days for control C57Bl6 mice, at 49–56 days for the presymptomatic mice and at 102–106 days (mean age of peak weight) for the disease-onset $SOD1^{G93A}$ mice, and at the presymptomatic age of 87–94 days for $SOD1^{G37R}$ mice. Busulfan was diluted in 0.9% NaCl and fractioned doses of 25 mg per kg were injected every day for four consecutive days for a total dose of 100 mg per kg per mouse. This dose was chosen following published data showing high myeloablation efficiency of this regimen without overall toxicity[56]. Moreover, the dose used was in the range showing no impact on the CNS[34,35]. For the irradiation control experiments, 49–56- day-old control C57Bl6 mice were irradiated with 5.25 Gy twice within 4 h (Faxitron, Edimex).

BM preparation and transplantation. Whole BM was extracted from the femurs and tibiae of age-matched donor mice ($SOD1^{G93A}$, actin–GFP, $SOD1^{WT}$/GFP or Nox2 KO mice). BM cells were resuspended in 0.1 M PBS at a final concentration of 5×10^4 cells per μl. A total of 5×10^6 cells were injected in the tail vein of recipient mice 24 h after irradiation or the final injection of busulfan. To control myeloablation efficiency, 100 μl of blood was collected from the retro-orbital sinus of every irradiated or busulfan-treated mouse before BM injection and mixed with 100 μl of HBSS and 1% FCS (Life Technologies). Red blood cells were lysed with 2 ml of fixative BD FACS lysing solution (BD Biosciences) for 15 min. The cells were centrifuged, resuspended in 100 μl of 0.1 M PBS and counted using a hemocytometer.

BM chimerism. For control experiments, chimerism was measured in the blood of irradiated or busulfan-treated and BM-grafted C57Bl6 mice every week until D40 (40 days after BM transplantation), and then every month until D370 after the transplantation by flow cytometry. In mutant SOD1 mice, chimerism was measured in the blood of $SOD1^{G37R}$-grafted mice at 12, 26, 33, 116, 152 and 278 days after BM transplantation by flow cytometry. For $SOD1^{G93A}$ mice, grafted at the presymptomatic stage, chimerism was measured 12 and 60 days after the graft by flow cytometry (for GFP and $SOD1^{WT}$/GFP BM grafts) or quantitative PCR (qPCR) (for Nox2 KO BM grafts). For mice grafted at onset, analysis was performed at 12 and 24 days after the transplantation by flow cytometry. To verify chimerism using flow cytometry, blood samples were collected from the retro-orbital sinus and treated as mentioned above for cytometry analyses. Myeloid cells were labeled with anti-CD11b-PE (1:200; BD Pharmingen) antibodies. Cytometry was performed using a Guava Easy Cyte mini flow cytometer (Millipore) to measure GFP and CD11b-PE, and data were analyzed using FlowJo software. Chimerism for mice grafted with Nox2 KO BM was indirectly measured on the basis of the level of human *SOD1* DNA content in blood cells. As blood cells from Nox2 KO mice did not carry the human *SOD1* transgene, decreased levels of human *SOD1* in the blood directly reflects the replacement of endogenous SOD1^{G93A} mouse blood cells by Nox2 KO mouse blood cells. Blood samples were collected from the retro-orbital sinus. DNA was extracted from total blood using a PureLink genomic DNA Minikit (Invitrogen, Life Technologies). qPCR was performed as described in ref. [3] using TaqMan probes and Light Cycler Probe Master Mix on a LightCycler 96 system (Roche Applied Biosystem). A total of 24 ng of DNA was used per reaction with primers at a final concentration of 0.5 μM. The specific primers and probes used are as follows: human *SOD1* forward, CAATGTGACTGCTGACAAAG; human *SOD1* reverse, GTGCGGCCAATGATGCAAT; human *SOD1* probe, fam-CCGATGTGTCTATTGAAGATTCTG; *Apob* forward, CACGTGGGCTCCAGCATT; *ApoB* reverse, TCACCAGTCATTTCTGCCTTTG; and *Apob* probe, Hex-CCAATGGTCGGGCACTGCTCAA. Each sample was run in triplicate, and the expression of human *SOD1* DNA was calculated using the ΔΔCt method, normalized to the mouse *Apob* gene and relative to the control samples from non-grafted SOD1^{G93A} mice.

***Cybb* mRNA levels in T lymphocytes.** *Cybb* mRNA expression levels were assessed in isolated mouse blood T lymphocytes and compared to blood monocytes that are known to express Nox2 as a positive control. Blood samples were collected from the retro-orbital sinus of symptomatic

SOD1^{G93A} mice and age-matched control C57Bl6 mice. Red blood cells were lysed using a non-fixative lysis buffer (BD Pharm Lyse, BD Biosciences, 1/10 in water). CD11b$^+$ cells were first isolated using an anti-CD11b microbead-coupled antibody and LS columns (Miltenyi Biotec) according to the manufacturer's instructions to obtain CD11b$^+$ cells in the positive selection and all the other cell types, including T cells, in the negative selection. In a second step, lymphocytes were isolated from the negative selection using a Pan T Cell Isolation kit II (Miltenyi Biotec). Briefly, non-T cells were labelled using biotin-conjugated antibodies against CD11b, CD11c, CD19, CD45R (B220), CD49b (DX5), CD105, Ter119 and MHC class II, and then coupled to magnetic beads using anti-biotin microbeads. Magnetic separation was performed using LS columns (Miltenyi Biotec), and the eluent contained purified T lymphocytes. T cell purity was verified by flow cytometry using an anti-CD3-PE antibody (1:200, BioLegend) on a FACS Verse Cytometer (BD Biosciences), and data were analyzed using FlowJo software. RNA from lymphocytes and CD11b$^+$ cells were extracted using a Nucleospin RNA XS kit (Macherey-Nagel). RNA concentrations were determined by TapeStation using the High sensitivity ScreenTape assay (Agilent). Reverse transcription was performed with Superscript IV (Life Technologies) using oligo dT and 10 ng of total RNA. qPCR was performed with SYBR Green Master Mix (Applied Biosystem) and 1 µl of 1:4 diluted cDNA. *Cybb*-specific primers were *Cybb* forward: ACTCCTTGGGTCAGCACTGG and *Cybb* reverse: GTTCCTGTCCAGTTGTCTTCG, and the specific primers for the normalizer TATA-box binding protein (*Tbp*) were forward: ACCTTATGCTCAGGGCTTGG and reverse: GGAGTAAGTCCTGTGCCGTA. Each sample was run in duplicate, and the relative expression of *Cybb* mRNA was determined using the $\Delta\Delta$Ct method and normalized to the *Tbp* mRNA expression level.

Mouse tissue collection. Mice were deeply anesthetized with xylazine (Rompun 0.2%) and ketamine (Imalgene 500) and transcardially perfused with 0.1 M ice-cold PBS followed by 4% paraformaldehyde (PFA) in phosphate buffer. Sciatic nerves, gastrocnemius muscles, lumbar and cervical spinal cords and brains were collected and post-fixed in 4% PFA for 4 h. Tissues were then cryoprotected in 30% sucrose in PBS for 48 h before freezing in isopentane at −40 °C.

Immunohistochemistry analyses. *Sciatic nerves.* Longitudinal cryosections (12 μm) were incubated in a blocking solution containing 0.1 M PBS, 0.3% Triton X-100 (PBST) and 3% BSA (Sigma Aldrich) for 1 h and stained overnight at 4 °C using the following monocyte/macrophage antibody markers in PBST: rat anti-CD11b (1:400, BD Biosciences); rat anti-CD68 (1:400, AbD Serotec); rat anti-F4/80 (1:100, AbD Serotec); chicken anti-GFP (1:800, Life Technologies); rabbit anti-RFP (1:500, Abcam); rat anti-CD3 (1:100, AbD Serotec); goat anti-Sox10 (1:50, R&D Systems); and rabbit anti-elastase (1:1,000, Abcam). Staining was revealed with an Alexa Fluor-594 or Alexa Fluor-488 fluorescent secondary antibody (1:1,000, Life Technologies).

Lumbar spinal cord sections. Transverse cryosections (30 μm) were incubated overnight at room temperature with the following antibodies in PBST: rabbit anti-Iba1 (1:500, Wako Chemicals); rat anti-CD169 (1:200, AbD Serotec); rat anti-CD3 (1:100, AbD Serotec); rat anti-CD4 (1:100, AbD Serotec); rat anti- CD8 (1:100, AbD Serotec); mouse anti-Ki67 (1:200, BD Pharmingen); goat anti-Iba1 (1:500, Abcam); chicken anti-GFP (1:800, Life Technologies); and rabbit anti-RFP (1:500, Abcam). The different stainings were revealed using species-specific Alexa Fluor-488, -594 or -647 secondary antibodies (1:1,000, Life Technologies). In nerves and spinal cords, the GFP signal from actin–GFP BM-grafted mice was assessed as a live GFP^{+} signal. $SOD1^{G37R}$ mouse sciatic nerve and spinal cord sections were stained with Sudan black (1% in 70% ethanol) following the secondary antibody to decrease lipofuscin autofluorescence.

Image acquisition. For mouse tissues, pictures of macrophage activation in the nerves (CD11b, CD68 and F4/80 staining), microglial activation (Iba1 staining), infiltration of GFP^+ peripheral cells in the spinal cord and $Ki67^+$ cells in the spinal cord were obtained using an Axioscan scanner (Zeiss) with Zeiss ZEN v.2 software. For colocalization analyses with sciatic nerve macrophages, pictures were obtained using a Leica TCS SP8 X confocal microscope with LAS X v.3 software. For all the other stainings of nerve, spinal cord and muscle sections, pictures were taken with an AxioImager Z1 microscope (Zeiss) with AxioVision v.4.8.2 software. All the analyses were performed using Fiji software (ImageJ).

Cell counts and cell activation. GFP^+ cell counts. The percentage of GFP^+ macrophages in the sciatic nerves of grafted mice was determined by counting cells positive for GFP and the macrophage markers CD11b, CD68 and F4/80 over the total number of macrophages ($CD11b^+CD68^+F4/80^+$ cells). Macrophages were counted from five to nine pictures taken randomly on each nerve section at a magnification of ×20. Countings were determined from 12-μm serial sections across the sciatic nerve in every eighth section corresponding to a total of four to six sections per animal. To calculate the percentage of GFP^+ macrophages in the lymph nodes of onset-grafted $SOD1^{WT}/GFP \rightarrow SOD1^{G93A}$ mice, lymph nodes (popliteal, inguinal and axillary) were taken from mice at the early-symptomatic stage. Lymph nodes were post-fixed for 4 h in 4% PFA and then cryopreserved in 30% sucrose before freezing. Transverse cryosections (12 μm) were stained for the different populations of lymph node macrophages based on ref. [57] using the following antibodies: goat anti-mouse MerTK (R&D Systems, BAF591, 1:500); rat anti-mouse F4/80 (Bio-Rad, MCA497R, 1:100); and rat anti-mouse CD169 (Bio-Rad, MCA947G, 1:100). Staining was revealed with donkey anti-rat Alexa-594 (Life Technologies, A-21209, 1:1,000) and donkey anti-goat Alexa-594 (Life Technologies, A-11058, 1:1,000). About 9–14 ×40 objective pictures of the lymph nodes were taken using a confocal microscope (SP8 Leica DSL, ×40 oil), and GFP^+ macrophages were counted over the entire population of macrophages (n = 3 mice, 710–1,272 macrophages counted per mouse). GFP^+ cell infiltration in the spinal cord was determined using two different measures: (1) the GFP immunoreactive area (the area occupied by GFP staining compared to the total area of the lumbar spinal cord parenchyma) using Fiji software; and (2) the percentage of GFP^+Iba1^+ microglial cells. A Fiji macro was designed to determine the total number of $Iba1^+$ microglial cells and GFP^+ cells in the parenchyma of each lumbar spinal cord section. A colocalization module was used to count double-positive ($Iba1^+$ and GFP^+) cells. Measurements were done on 30-µm serial sections across the entire lumbar spinal cord and counted in every 24th stained section corresponding to a total of 9–11 sections per animal.

T cell counts. T lymphocyte ($CD3^+$ cell) numbers were determined manually. Counting was performed using an AxioImager Z1 microscope (Zeiss). To determine $CD4^+$ and $CD8^+$ T-cell-subtype proportions, a sequential double-staining protocol was performed in which labeling of $CD4^+$ or $CD8^+$ T lymphocytes was performed first using a rat-anti CD4 antibody (1:100, AbD Serotec) or a rat-anti CD8 antibody (1:100, AbD Serotec), respectively, and the staining revealed by an Alexa Fluor-594 fluorescent secondary antibody (1:1,000, Life Technologies). In a second step, all the T lymphocytes were labeled using a rat-anti $CD3^+$ antibody (1:100, AbD Serotec), and revealed by an Alexa Fluor- 488 fluorescent secondary antibody (1:1,000, Life Technologies). All the $CD3^+$ cells and the co-labeled $CD3^+CD4^+$ T lymphocytes were counted in parallel, and the CD4/CD8 T-cell proportion was calculated. The number of $Foxp3^+$ Treg cells was determined in the spinal cord of non-grafted $SOD1^{G93A}$ mice at disease onset and at end-stage, and in onset-grafted $SOD1^{G93A}{\rightarrow}SOD1^{G93A}$ and $SOD1^{WT}$/GFP$\rightarrow SOD1^{G93A}$ mice at the early-symptomatic stage and end-stage. To count $Foxp3^+$ Treg cells, antigen retrieval was performed on floating spinal cord sections using target antigen retrieval (Dako, S169984-2) according to manufacturer's instructions. T_{reg} cells were labeled for the pan-T-cell marker CD3 with a rabbit anti-mouse CD3 antibody (Abcam, ab16669, 1:100) and for the T_{reg} cell marker Foxp3 with a rat anti-mouse Foxp3 antibody (Life Technologies, 14-5773-82, 1:100) overnight. Stainings were revealed using a goat anti-rat Alexa Fluor-594 (Life Technologies, 1:1,000) and a goat anti-rabbit Alexa fluor-488 (Life Technologies, 1:1,000). Both $CD3^+Foxp3^+$ and $CD3^+Foxp3^-$ cells were manually counted using an AxioImager Z1 (Zeiss) microscope. All the quantifications were performed in the parenchyma of every 24th 30-μm serial lumbar spinal cord section corresponding to a total of 9–11 sections per animal.

Sciatic nerve macrophage and spinal cord microglial activation. Peripheral macrophages were stained for CD11b, CD68 and F4/80 markers, as expression levels were higher in these cells than for Iba1, while microglial cells were stained for Iba1, which is highly expressed in microglial cells. Sciatic nerve and spinal cord sections were imaged using an AxioScan Z1 (Zeiss) microscope. A scan protocol was set up to keep the same parameters (time and intensity of exposure and focus strategy) for every sciatic nerve section and every spinal cord section, and only coarse and fine focuses were adapted to each slide. Fiji software was used to measure sciatic nerve macrophage activation and numbers (entire sciatic nerve longitudinal sections were analyzed) as follows: (1) for the fluorescent immunoreactive area occupied by the macrophage markers CD11b, CD68 and F4/80, a common threshold for every section was set up, and the percentage area was measured; and (2) for the number of macrophages ($CD11b^+CD68^+F4/80^+$ cells per mm^2), a macro was set up using Fiji to isolate and count every macrophage on the section. Measurements were made from every 8th 12-μm sciatic nerve section, which corresponded to a total of 4–6 sections per animal. Fiji software was used to measure spinal cord microglial activation (the entire spinal cord section was analyzed) as follows: a common microglial-cell-detection threshold was set up for every section, and the percentage area (measuring the Iba1$^+$ fluorescent immunoreactivity area in the parenchyma) was calculated. Measurements were made from every 24th 30-μm lumbar spinal cord section, which corresponded to a total of 9–11 sections per animal.

Ccr2 reporter mice to assess tissue infiltration. To determine Ccr2 monocyte/ macrophage infiltration in Ccr2–GFP×SOD1^{mutant} mouse sciatic nerve or spinal cord, sections were stained with chicken anti-GFP antibodies (1:800, Life Technologies). Of note, although Ccr2 is supposed to be downregulated during macrophage differentiation, in this Ccr2–GFP mouse line, the GFP protein was still present in differentiated macrophages (likely linked to the stability of GFP compared to the promoter activity), which represented an advantage for detecting cells infiltrating the CNS. We performed two independent measurements: (1) double-positive Ccr2–GFP$^+$/Iba1$^+$ cells were manually counted in Ccr2– GFP×SOD1^{mutant} mouse tissues; and (2) spinal cord sections previously stained using anti-Iba1 and anti-GFP (Ccr2 cells) were scanned. The number of Iba1$^+$ microglial cells was counted using Fiji software and a designed macro. For each spinal cord section, the number of Ccr2$^+$ cells previously counted (and shown in Extended Data Fig. 5i,j, green bars) are related to the total number of Iba1$^+$ microglial cells (counted by the macro), thereby giving a percentage of Iba1$^+$ cells expressing Ccr2 (by GFP). This quantification could not be performed for CCR2–RFP×SOD1 mice since the anti-RFP antibody was made from rabbit, as is our anti-Iba1 antibody. Therefore, co-staining could not be performed, and the quantification explained above was not possible. In Ccr2–RFP×SOD1^{mutant} mice, most of the RFP$^+$ (Ccr2-expressing) cells were CD3$^+$. We could not perform triple staining with microglial/macrophage markers since the anti-RFP antibody was made from rabbit (as is our anti-Iba1 antibody), and the T lymphocyte marker CD3 or the macrophage markers CD11b, CD68 and F4/80 were all rat antibodies. Thus, we chose to perform double staining using rabbit anti-RFP (for $Ccr2^+$ cells) (1:500, Abcam) and rat anti-CD3 antibodies (1:100, AbD Serotec) to count double-positive $Ccr2^+CD3^+$ cells that were much more numerous, while $Ccr2^+CD3^-$ cells were considered as monocyte/macrophage-infiltrated cells.

MN counts. MN numbers were determined from 30-μm serial sections across the entire lumbar spinal cord, and counted in the ventral horn spinal cord sections, in every 12th cresyl-violet-acetate-stained section. This corresponded to a total of 18–22 sections per animal for $n = 3–9$ animals per genotype and time point.

Neuropathology of spinal cord and nerve sections from patients with ALS. Patients with ALS were enrolled in the NeuroCEB (Neurologie-Collection d'Echantillons Biologiques) brain and spine donation program declared to the 'Ministry of Research and Universities', as requested by French law. An explicit consent form was signed by the patient him/herself or by the next of kin in the name of the patient in accordance with the French Bioethical Laws. Clinical data of the 11 patients and 4 controls are provided in Supplementary Table 1. Patients with ALS included 9 men and 2 women aged 38–73 years, and controls included 2 men and 2 women aged 45–73 years. Three levels of spinal cord (cervical, thoracic and lumbar) and brachial nerve tissues were taken. Slides were stained with hematoxylin and eosin and Luxol fast blue. Immunostainings were performed after deparaffinization by an automatic slide stainer (Benchmark XT Ventana staining system). Slides were pretreated at 95 °C in CC1 (pH 8) retrieval buffer (Ventana Medical Systems). The 5-μm thick sections were immunolabeled with anti-CD68 antibody (mouse monoclonal, clone KP1, Dako, 1:1,000). Mouse IgG was detected with a biotin-free detection system (Ventana Medical Systems Ultraview Universal DAB Detection kit).

RNA-seq. *Isolation of microglia from mouse spinal cord and macrophages from mouse sciatic* *nerves.* Microglial cells were isolated from the spinal cords of SOD1^{G93A} mice at the following different disease stages: presymptomatic (mean age of 50.8 days), onset (mean age of 105 days), early symptomatic (mean age of 152.6 days) and end-stage (mean age of 169.4 days). Microglial cells were not isolated from the late-symptomatic stage since some infiltrated monocyte/macrophage cells were present in the spinal cord. Microglial cells were also isolated from C57Bl6 (Bl6) mice and SOD1^{WT} mice at the mean age of disease onset (109.8 days for Bl6 and 107.3 days for SOD1^{WT}) and at the mean age of disease end-stage (165.6 days for Bl6 and 165.4 days for SOD1^{WT}). Sciatic nerve peripheral macrophages were isolated from SOD1^{G93A} mice at the presymptomatic stage, onset, early symptomatic and disease end-stage. Sciatic nerve macrophages could not be isolated from Bl6 sciatic nerves (probably linked to their very low numbers in noninflammatory conditions), but could be recovered from SOD1^{WT} mice at the age corresponding to disease end-stage (most likely linked to the increased number of cells that reached a density comparable to that of SOD1^{G93A} at disease onset; Fig. 1f, Supplementary Fig. 2a, Extended Data Fig. 9a and Supplementary Table 2). Spinal cord microglial cells and sciatic nerve macrophages were also isolated from onset-grafted SOD1^{G93A}→SOD1^{G93A} and SOD1^{WT}/GFP→SOD1^{G93A} mice at the early-symptomatic stage (defined by 35% of grip strength loss) and disease end-stage. Mice were all females and were deeply anesthetized using xylazine (Rompun 0.2%) and ketamine (Imalgene 500) and transcardially perfused with ice-cold 0.1 M PBS. Two whole left and right sciatic nerves (from the gastrocnemius muscles to the spine vertebrae) were collected and pooled, except for the macrophages at the presymptomatic stage, where four sciatic nerves from two mice of the same age were needed to recover enough cells, and whole spinal cords were flushed using 0.1 M PBS. Tissues were chopped in DMEM-F10 (1:1, Life Technologies) culture medium supplemented with 10% FCS (low endotoxins, Life Technologies). Tissues were passed through a 100-µm nylon filter (Falcon). Myelin was removed using a Percoll gradient (30–37–70% Percoll, GE Healthcare) in 0.1 M PBS. The entire procedure was performed at 4 °C and did not use enzymatic digestion/incubation at 37 °C; this was to avoid ex vivo activation of the cells. Briefly, 1.6 ml of 70% Percoll solution was laid at the bottom of 5-ml polypropylene tubes (Falcon) and then gently covered by 1.6 ml of 37% Percoll. Cells were homogenized in 30% Percoll solution and carefully laid on top and centrifuged (without break) for 40 min at 800 *g* at 4 °C. The 30% Percoll layer containing myelin was removed, and cells were recovered at the interface between the 37% and the 70% Percoll layers. Cells were resuspended in 0.1 M PBS, 0.5% BSA (Sigma Aldrich), 2 mM EDTA (Life Technologies). Microglial cells or macrophages were isolated using an anti-CD11b magnetic microbead-coupled antibody and MS columns (Miltenyi Biotec) according to manufacturer's instructions. Between 1.0×10^5 and 1.8×10^5 microglial cells were recovered from spinal cords (one spinal cord from one animal per sample; Supplementary Table 2), and between 3×10^4 and 5×10^4 macrophages were recovered from sciatic nerves (two sciatic nerves from one animal per sample, except for the presymptomatic stage, whereby four sciatic nerves from two mice were pooled, Supplementary Table 2), depending on the genotype and disease stage of the mice. For RNA isolation, cells were centrifuged at 300 *g* at 4 °C and kept at −80 °C until further use. For quality control, cells were resuspended in 0.1 M PBS, 0.5% BSA (Sigma Aldrich), 2 mM EDTA (Life Technologies), 1:200 Fc Block (anti-CD16/CD32, BD Biosciences), and 50 µl was used per well for cytometry analysis. Cell viability was controlled with 7-amino-actinomycin D (7-AAD) viability staining solution (50 µg ml^{-1}, BioLegend) according to the manufacturer's instructions, and cell purity was assessed using anti-CX3CR1-FITC (1:50, R&D Systems) and anti-F4/80-APC (1:200, BioLegend) antibodies. Cytometry was performed using a FACS Verse cytometer (BD Biosciences), and data were analyzed using FlowJo software.

RNA extraction and sample preparation for RNA-seq. RNA was extracted from spinal cord microglial cells and from sciatic nerve macrophages using a Nucleospin RNA XS kit (Macherey Nagel) with a final RNA elution in 10 µl. Microglial cell RNA concentration was determined using a RNA 6000 Pico kit (Agilent Technologies) on an Agilent Bioanalyzer. Although the number of microglial cells and macrophages, and therefore the total quantity of RNA obtained from the two cell populations, were different, to compare microglial cells and macrophages, we used the same protocol and the same kits; therefore, we used only a fraction of the microglial RNA obtained. A total of 1 ng of microglial cell RNA (from a total RNA amount of 15–70 ng per microglial sample) and total RNA of sciatic nerve macrophages (RNA quantities for macrophages were too low to be measured, but were estimated from the number of cells in comparison to microglia) were used to perform cDNA synthesis using a Smart-Seq v4 Ultra Low Input RNA kit for sequencing (Clontech Laboratories) with linear pre-amplification. Library preparation was made with 150 pg of amplified cDNA for every sample (microglia and macrophages) using a Nextera XT DNA Library Preparation kit (Illumina). Eight samples were run with a 400 million cartridge to reach an average coverage of 50 million reads per sample (75 bp, paired-ends). Sequencing was performed using a NextSeq 500 high Output Kit V2 on a NextSeq 500 sequencer (Illumina). Library preparations and sequencing were performed by the ICM iGenSeq core facility.

RNA-seq data analysis. RNA-seq data analysis was performed by GenoSplice (http://www.genosplice.com). Sequencing, data quality, reads repartition (for example, for potential ribosomal contamination) and insert size estimation were performed using FastQC (v.0.11.2), Picard-Tools (v.1.119), Samtools (v.1.0) and rseqc (v.2.3.9). All the samples presented and used for the analyses passed all the quality controls. Reads were mapped using STAR (v.2.4.0)[58] on the mm10 Mouse genome assembly. Gene expression regulation studies were performed as previously described[59]. Briefly, for each gene present in the mouse FAST DB v2018_1 annotations, reads aligning on constitutive regions (which are not prone to alternative splicing) were counted. Based on these read counts, normalization and differential gene expression were performed using DESeq2 (ref. [60]) on R (v.3.5.3). Only genes expressed in at least one of the compared experimental conditions were further analyzed. Genes were considered as expressed if their reads per kilobase of transcript per million (RPKM) value was greater than 96% of the background RPKM value based on intergenic regions. Results were considered statistically significant for P values ≤ 0.05 and fold-changes ≥ 1.5. Enrichment analysis was performed using Database for Annotation, Visualization and Integrated Discovery (DAVID) v.6.8. Additional analyses were performed using R v.3.5.3 software and IPA v.52912811 (IPA, Qiagen).

Statistics and reproducibility. All manual counts were performed in a blinded manner. Non-objective computational measurements such as immunofluorescence quantification by scanning devices did not require blinding. A total of 14 mice were excluded from our cohorts of grafted mice due to either major weight loss due to malocclusion ($n = 8$ mice) and the need to euthanase them or, in rare cases, ($n = 6$ mice) premature death due to failure of BM grafting. Beside these mice, no data were excluded from analysis. All data are presented as the mean ± s.e.m., and the statistics were performed using GraphPad software Prism 7. No statistical methods were used to predetermine sample sizes, but our sample sizes were similar to those reported in previous publications[3,55]. Sample sizes for all animal cohorts were determined according to published guidelines for working with ALS mouse models[61]. Data distribution was assumed to be normal, but this was not formally tested. Regarding randomization, for experiments using post-mortem tissues, randomization was not applicable since only one test group, corresponding to patient tissues or controls stained with the same antibodies, was used. All other experiments used mice. Mice were randomly assigned to experimental time points. One-way analysis of variance

(ANOVA) followed by Tukey's post hoc analysis of mean differences was used to compare multiple groups; one-way ANOVA followed by Dunnett's post hoc analysis was used to compare each mean to a control mean; Student's *t*-tests, two-tailed and unpaired, were used to compare means of two groups and log-rank tests were performed to analyze survival curves. For RNA-seq data, gene deregulation *P* values were obtained with a two-sided Wald test (with the DESeq2 package from R), and adjusted *P* values were calculated using Benjamini–Hochberg correction. Enrichment analysis *P* values were calculated with the EASE score: one-sided modified Fisher exact test from DAVID v.6.8 or a right-tailed Fisher exact test from IPA software. Regarding replication, every mouse and patient/control individual represents a replicate, and the number of replicates is mentioned for each experiment in the figure legend and/or Supplementary Table 7. Additional information on statistics (sample sizes, tests and *P* values) are provided in Supplementary Table 7.

Reporting Summary. Further information on research design is available in the Nature Research Reporting Summary linked to this article.

Data availability

The raw RNA-seq data were uploaded to the NCBI GEO under the accession code GSE156202.

Life Science Reporting Summary: Reporting Summary. Further information on research design is available in the Nature Research Reporting Summary linked to this article.

References

51. Van Hove, H. *et al.* A single-cell atlas of mouse brain macrophages reveals unique transcriptional identities shaped by ontogeny and tissue environment. *Nat. Neurosci.* **22**, 1021–1035 (2019).

52. Saederup, N. *et al.* Selective chemokine receptor usage by central nervous system

myeloid cells in CCR2-red fluorescent protein knock-in mice. *PLoS One* **5**, e13693 (2010).

53. Lund, H. *et al.* Competitive repopulation of an empty microglial niche yields functionally distinct subsets of microglia-like cells. *Nat. Commun.***9** (2018)
54. Gosselin, D. *et al.* An environment-dependent transcriptional network specifies human microglia identity. *Science* **356**, 33–35 (2017).
55. Jaarsma, D. *et al.* Human Cu/Zn superoxide dismutase (SOD1) overexpression in mice causes mitochondrial vacuolization, axonal degeneration, and premature motoneuron death and accelerates motoneuron disease in mice expressing a familial amyotrophic lateral sclerosis mutant SO. *Neurobiol. Dis.* **7**, 623–43 (2000).
56. Pollock, J. D. *et al.* Mouse model of X–linked chronic granulomatous disease, an inherited defect in phagocyte superoxide production. *Nat. Genet.* **9**, 202–209 (1995).
57. Serbina, N. V., Hohl, T. M., Cherny, M. & Pamer, E. G. Selective Expansion of the Monocytic Lineage Directed by Bacterial Infection. *J. Immunol.* **183**, 1900–1910 (2009).
58. Mesci, P. *et al.* System xC is a mediator of microglial function and its deletion slows symptoms in amyotrophic lateral sclerosis mice. *Brain* **138**, 53–68 (2014).
59. Westerhof, G. R. *et al.* Comparison of Different Busulfan Analogues for Depletion of Hematopoietic Stem Cells and Promotion of Donor-Type Chimerism in Murine Bone Marrow Transplant Recipients. *Cancer Research*. **60**, 5470–5478 (2000).
60. Baratin, M. *et al.* T Cell Zone Resident Macrophages Silently Dispose of Apoptotic Cells in the Lymph Node. *Immunity* **47**, 349–362 (2017).
61. Dobin, A. *et al.* STAR: Ultrafast universal RNA-seq aligner. *Bioinformatics* **29**, 15–21 (2013).
62. Noli, L., Capalbo, A., Ogilvie, C., Khalaf, Y. & Ilic, D. Discordant Growth of

Monozygotic Twins Starts at the Blastocyst Stage: A Case Study. *Stem Cell Reports* **5**, 946–953 (2015).

63. Love, M. I., Huber, W. & Anders, S. Moderated estimation of fold change and dispersion for RNA-seq data with DESeq2. *Genome Biol.* **15**, 1–21 (2014).

64. Ludolph, A. C. *et al.* Guidelines for the preclinical in vivo evaluation of pharmacological active drugs for ALS/MND: Report on the 142nd ENMC international workshop. *Amyotroph. Lateral Scler.* **8**, 217–223 (2007).

Supplementary Information

Patients #	Etiology	Mutation	Gender	Age of Onset (in years)	Site of onset	Survival (in months)	Age of death
1	FALS	SOD1 A4T	Female	45	Lower limbs	17	47
2	FALS	SOD1 G93D	Male	34	Lower limbs	48	38
3	FALS	SOD1 D83G	Male	72	Upper limbs	7	73
4	FALS	TARDBP G348V	Male	43	Upper limbs	39	47
5	FALS	TARDBP G295S	Female	58	Lower limbs	116	68
6	FALS	UBQLN2 P506A	Male	45	Lower limbs	46	49
7	FALS	C9orf72 Repeat expansion	Male	53	Bulbar	20	55
8	SALS	None	Male	37	Bulbar	29	39
9	SALS	None	Male	38	Lower limbs	81	45
10	SALS	None	Male	52	Upper limbs	124	62
11	SALS	None	Male	56	Upper limbs	37	59
12	Control	NA	Female	NA	NA	NA	45
13	Control	NA	Male	NA	NA	NA	63
14	Control	NA	Male	NA	NA	NA	61
15	Control	NA	Female	NA	NA	NA	61

Supplementary Table 1 | ALS patient clinical data (associated to Fig. 1 and Extended Data Fig. 1). FALS: familial ALS, SALS: sporadic ALS, None: no mutation identified after genetic analysis of *C9orf72*, *SOD1*, *TARDBP*, *FUS* and *UBQLN2*. NA: Not applicable.

		Mean cell numbers +/- SEM (n)			
Cell type	Genotype	Pre-sympt.	Onset	Early Sympt.	End-stage
Macrophages	$SOD1^{G93A}$	33’189 +/- 1’646 (n=3) §	32’844 +/- 1’479 (n=3)	40’326 +/- 4’855 (n=4)	50’705 +/- 898 (n=4)
	$SOD1^{WT}$				31’762 +/- 2’985 (n=4)
	$SOD1^{WT}$-> $SOD1^{G93A}$			42'091 +/- 2’003 (n=2)	38'196 +/- 1’112 (n=3)
	$SOD1^{G93A}$-> $SOD1^{G93A}$			34'376 +/- 6’194 (n=3)	34’623 +/- 11'879 (n=3)
Microglia	$SOD1^{G93A}$	113’456 +/- 7’395 (n=4)	112’523 +/- 9’412 (n=5)	164’831 +/- 8’168 (n=4)	184’204 +/- 9’699 (n=4)
	$SOD1^{WT}$		125’766 +/- 8’574 (n=4)		118’301 +/- 2’427 (n=4)
	Bl6		109’019 +/- 4’138 (n=4)		106’568 +/- 5’137 (n=4)
	$SOD1^{WT}$-> $SOD1^{G93A}$			123'131 +/- 27’913 (n=3)	181'892 +/- 11'277 (n=3)
	$SOD1^{G93A}$-> $SOD1^{G93A}$			140' 280 +/- 53'853 (n=3)	138'734 +/- 48’412 (n=3)

Supplementary Table 2 | Mean numbers of peripheral nerve macrophages and microglia isolated using our protocol in each condition (associated to Figs. 6, 7, Extended Data Figs. 9, 10 and Supplementary Fig. 2). Mean numbers of microglial cells recovered from one mouse spinal cord and mean numbers of peripheral nerve macrophages isolated from 2 sciatic nerves of one mouse except for the pre-symptomatic stage (§) where 4 sciatic nerves from two mice had to be pooled to recover enough cells.

Supplementary Table 3 | Lists of sciatic nerve peripheral macrophage regulated genes over the disease course in SOD1^{G93A} mice. Lists of genes that are differentially expressed in sciatic nerve peripheral macrophages between two disease stages. Up-regulated genes are indicated in yellow, and down-regulated genes in purple. Normalized gene expression values of each condition are indicated in the last columns. Genes to be compared were selected if their differential expression reached a fold change of at least 1.5 and an adjusted p-value ≤ 0.05. p-values were obtained with a two-sided Wald test (performed with DESeq2 R-package) – listed in column 5; adjusted p-values were calculated using Benjamini and Hochberg correction – listed in column 6.

Supplementary Table 4 | Lists of spinal cord microglia regulated genes over the disease course in SOD1^{G93A} mice. Lists of genes that are differentially expressed in spinal cord microglial cells between two disease stages. Up-regulated genes are indicated in yellow, and down-regulated genes in purple. Normalized gene expression values of each condition are indicated in the last columns. Genes were considered regulated if their differential expression reached a fold change of at least 1.5 and an adjusted p-value ≤ 0.05. p-values were obtained with a two-sided Wald test (performed with DESeq2 R-package) – listed in column 5; adjusted p-values were calculated using Benjamini and Hochberg correction – listed in column 6.

Supplementary Table 5 | Lists of sciatic nerve peripheral macrophage compared to spinal cord microglia regulated genes. Lists of genes that are differentially expressed between microglial cells and macrophages at each disease stage. Up-regulated genes are indicated in yellow, and down-regulated genes in purple. Normalized gene expression values of each condition are indicated in the last columns. Genes were considered regulated if their differential expression reached a fold change of at least 1.5 and an adjusted p-value ≤ 0.05. p-values were obtained with a two-sided Wald test (performed with DESeq2 R-package) – listed in column 5; adjusted p-values were calculated using Benjamini and Hochberg correction – listed in column 6.

Supplementary Table 6 | Lists of sciatic nerve peripheral macrophage or microglial cell regulated genes in SOD1^{WT}->SOD1^{G93A} vs SOD1^{G93A}->SOD1^{G93A} onset grafted mice at the early symptomatic stage or disease end-stage. Lists of genes that are differentially expressed in sciatic nerve peripheral macrophages or microglial cells between onset grafted SOD1^{WT}->SOD1^{G93A} and SOD1^{G93A}->SOD1^{G93A} mice at the two disease stages of early symptomatic or end-stage. Up-regulated genes are indicated in yellow, and down-regulated genes in purple. Normalized gene expression values of each condition are indicated in the last columns. Genes were considered regulated if their differential expression reached a fold change of at least 1.5 and an adjusted p-value ≤ 0.05. p-values were obtained with a two-sided Wald test (performed with DESeq2 R-package) – listed in column 5; adjusted p-values were calculated using Benjamini and Hochberg correction – listed in column 6.

Supplementary Table 7 | Addiational informations on Statistics: Sample size related to Figs. 1-7, Extended Data Figs. 1-10, Supplementary Figs. 1, 2 and statistical data related to Figs.1-7, Extended Data Figs. 3, 6-8, Supplementary Fig. 2 and Supplementary Tables 3-6.

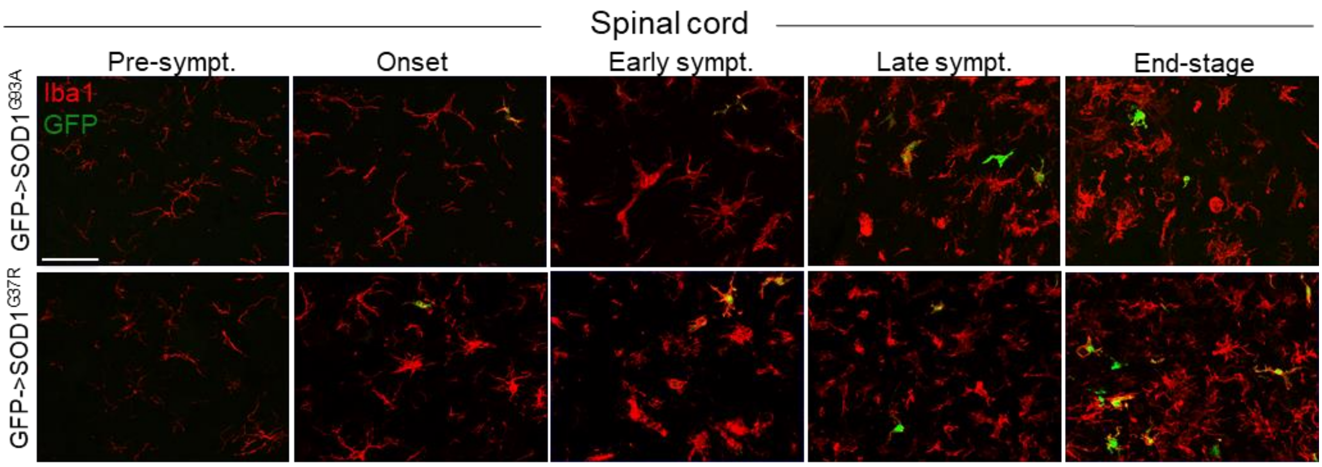

Supplementary Fig. 1 | Additional higher magnification pictures of GFP+ peripheral cell infiltration in the spinal cord. (Additional data to Fig. 2). Lumbar spinal cord sections of GFP->SOD1^{G93A} and GFP->SOD1^{G37R} mice at the different disease stages showing Iba1+ microglial cells (red) and GFP+ cells originating from the periphery (green). n=4 mice/group except n=5 for GFP->SOD1G93A at End-stage. Scale bar: 100µm.

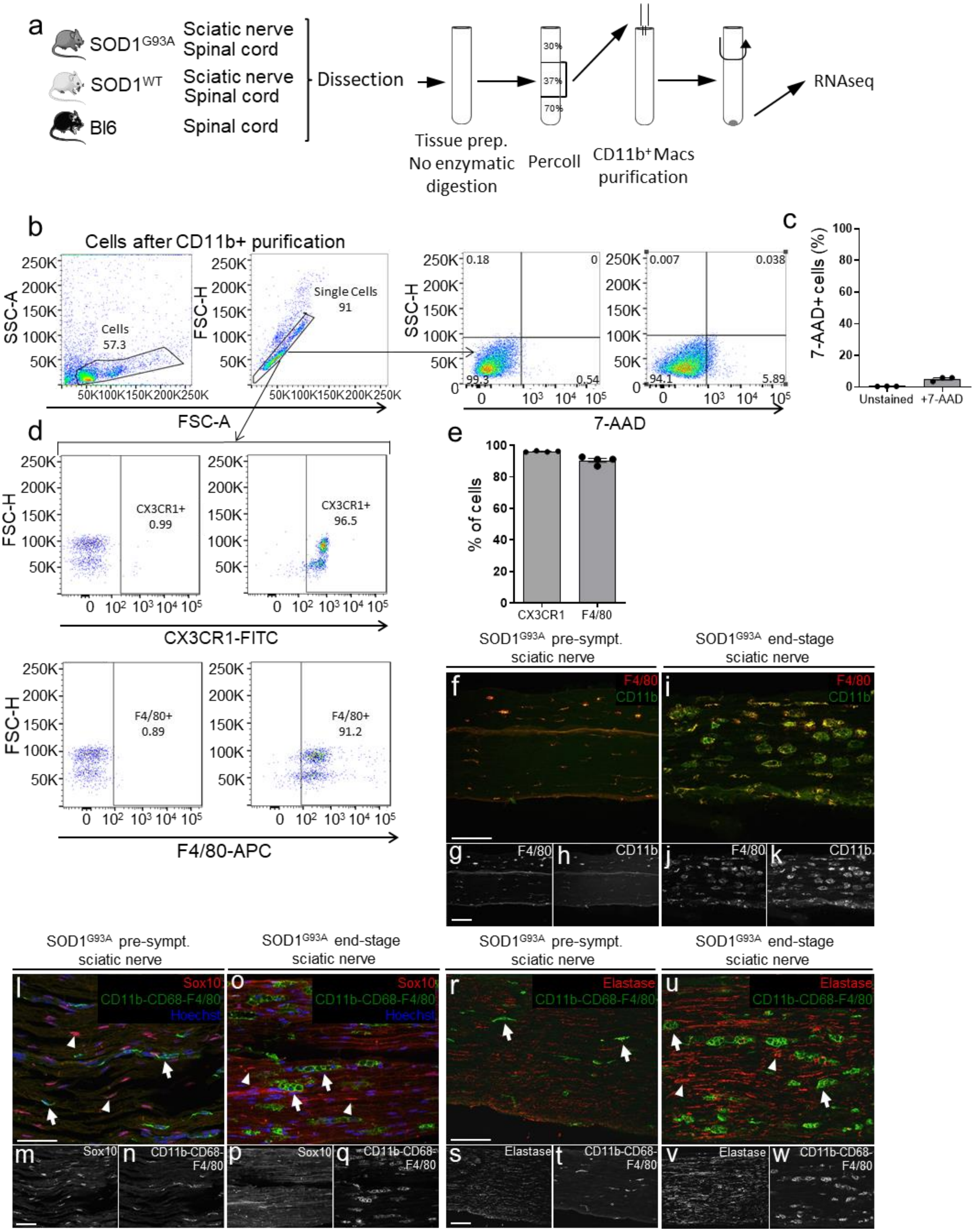
a
SOD1G93A
Sciatic nerve
Spinal cord
SOD1WT
Sciatic nerve
Spinal cord
Bl6
Spinal cord
Dissection
Tissue prep.
No enzymatic
digestion
Percoll
CD11b+ Macs
purification
RNAseq
b
Cells after CD11b+ purification
Cells
57.3
Single Cells
91
SSC-A
FSC-H
SSC-H
FSC-A
7-AAD
c
7-AAD+cells (%)
Unstained
+7-AAD
d
CX3CR1+
0.99
CX3CR1+
96.5
CX3CR1-FITC
F4/80+
0.89
F4/80+
91.2
F4/80-APC
e
% of cells
CX3CR1
F4/80
SOD1G93A pre-sympt.
sciatic nerve
SOD1G93A end-stage
sciatic nerve
F4/80
CD11b
Sox10
CD11b-CD68-F4/80
Hoechst
Elastase

Supplementary Fig. 2 | Purity of microglial cells and sciatic nerve peripheral macrophages for RNAseq analyses. (Additional data to Figs. 6-7 and Extended Data Figs. 9-10). **a**, Microglial cells and macrophages were isolated respectively from one mouse spinal cord and two mouse sciatic nerves or four sciatic nerves pooled from two mice for the pre-symptomatic time point. No enzymatic treatment was used for tissue preparation to avoid cell activation. Percoll gradient isolated leukocytes were subjected to CD11b+ microglia/macrophage purification. Mouse groups and sample numbers are shown in Extended Data Fig. 9a. **b-c**, Cytometry analysis (**b**: plots, **c**: quantification) of apoptotic cells using the 7-AAD marker, showing a low rate of mortality with the experimental procedure we used. Note that the cells isolated for the viability assay went through FACS procedure, which the cells isolated for RNAseq analysis did *not* go through, therefore we possibly overestimated the number of dying cells. Bars represent means +/- SEM for n=3 mice. **d**, Purity of MACS isolated $CD11b^+$ cells from the spinal cord of $SOD1^{G93A}$ mice at disease end-stage was analyzed with the microglial/macrophage markers CX3CR1 (upper panels) and F4/80 (lower panels) by flow cytometry. Percentage of positive cells (right) was determined according to isotype positivity threshold (left) and gating strategy is shown in **b**. **e**, Quantification of CD11b+ MACS-isolated cells expressing CX3CR1 and F4/80. Bars represent means +/- SEM for n=4 mice, for each marker. **f-k**, $SOD1^{G93A}$ pre-symptomatic (**f-h**) and end-stage (**i-k**) $SOD1^{G93A}$ mouse sciatic nerves immunostained first for the macrophage marker F4/80 (**f** and **i**, in red and **g**, **j**) and then the monocyte/macrophage marker CD11b (**f** and **i**, in green, and **h**, **k**) showing that all the CD11b+ cells in the sciatic nerve of $SOD1^{G93A}$ mice are F4/80+ monocyte/macrophages. **l-q**, pre-symptomatic (**l-n**) and end-stage (**o-q**) $SOD1^{G93A}$ mouse sciatic nerves co-immunostained for the macrophage markers CD11b-CD68-F4/80 (**l** and **o**, in green and **n**, **q**), the Schwann cell marker Sox10 (**l** and **o**, in red, and **m**, **p**) and nuclei with Hoechst (**l** and **o**, in blue). Macrophages (arrows) and Sox10+ cells (arrow heads) are not colocalized in sciatic nerves at both time points. **r-w**, $SOD1^{G93A}$ pre-symptomatic (**r-t**) and end-stage (**u-w**) $SOD1^{G93A}$ mouse sciatic nerves co-immunostained for the neutrophil marker elastase (**r** and **u**, in red and **s**, **v**) and for the macrophage markers CD11b-CD68-F4/80 (**r** and **u**, in green, and **t**, **w**). Neutrophils (arrow heads) are barely present at the pre-symptomatic stage and are not colocalized with macrophage markers (arrow) at both stages. n=4 mice at the pre-symptomatic stage and end-stage (for **f-w)**. Scale bars: 50 μm.